Species Dependence of pMDI/Wood Adhesion

by

Michael J. Malmberg

A Thesis submitted to the Faculty of
Virginia Polytechnic Institute and State University
in partial fulfillment of the requirement for the degree of

MASTERS OF SCIENCE

in

Wood Science and Forest Products

Approved by:

_____
C. E. Frazier, Chairman

_____ _____
W.G. Glasser R. H. Helm

December 5, 2000
Blacksburg, Virginia

Keywords: Fracture Mechanics, Wood Adhesion, NMR, FTIR, isocyanate

Species Dependence of pMDI/Wood Adhesion

by

Michael J. Malmberg

Wood Science and Forest Products

ABSTRACT

Polymeric methylenebis(phenylisocyanate) (pMDI) has increasingly been used in the wood particulate composite industry. Wood composites, especially oriented strand board (OSB) are made with many variations of wood species. Little research has been done to investigate how pMDI adhesion has been affected by species.

The present is divided into two parts. First, mode I fracture mechanics and surface free energy analysis was performed to investigate differences in adhesion between southern yellow pine and yellow-poplar bonded with pMDI. Secondly, an improvement in the synthesis of ^{13}C, ^{15}N labeled pMDI is discussed.

Mode I fracture results show that pMDI adhesion was affected differently by southern yellow pine compared yellow poplar. The shear energy release rate was significantly higher in pine/pMDI composites than in yellow poplar/pMDI composites. The total surface energy of southern yellow pine was shown to be significantly greater than yellow poplar. The free energy of adhesion (ΔG) of the pine/pMDI and the poplar/pMDI was investigated. The ΔG indicated that the pine/pMDI system would take more energy to separate compared to the poplar/pMDI system. Lastly, a double-labeled ^{13}C, ^{15}N pMDI adhesive was successfully synthesized to produce Solid-State NMR composites.

ACKNOWLEDGEMENTS

I would like to first thank Chip Frazier for the opportunity to study at Virginia Tech. He gave me a great opportunity to work with incredible personnel at a great facility. Secondly, I would like to thank Julie Krusch for her support and companionship during the most trying time of my entire life. I could not of kept my sanity or focus on my research after my divorce without her aid. Next I would like to thank my father Wally Malmberg for his encouragement and belief in me during my college years. Every time I would have liked to quit his disappointment would have been more than I could have handled. Lastly, I would thank my wife Lynn for giving me a life worth living and teaching me what life is about. Having her love, support and family around me has completely changed my focus in life and made me a better person. I would not have finished my corrections to attain my M.S. after leaving Tech without the life she has given me.

TABLE OF CONTENTS

LIST OF FIGURES

LIST OF TABLES

CHAPTER 1

INTRODUCTION----------

Particulate composites such as oriented strand board (OSB) have become increasingly important to society. This trend will continue as timber resource availability decreases. Polymeric methylenebis(phenylisocyanate) (pMDI) and phenol-formaldehyde (PF) are the major adhesives used in OSB manufacture. Polymeric MDI use has increased because pMDI bonded wood panels have certain production and performance advantages over PF bonded panels. Some of these advantages include shorter press times, lower resin loading, higher moisture tolerance, no formaldehyde emissions, and better strength and durability (1-6).

Historically, pMDI has not been formulated for specific wood composites because its manufacture feeds several higher value markets, and therefore very little process variation is possible. PMDI consists of approximately 50% of the 4,4'-monomer together with higher weight, methylene-bridged polyphenyl polyisocyanates (7) (Figure 1.1). Five to ten percent of the monomer fraction usually consists of the 2,4'-isomer and a very small amount (<1%) consists of the 2,2'-isomer (7). Industrial pMDI molecular weights are approximately 310 g/mole, number average (M_n), 380 g/mole, weight average (M_w).

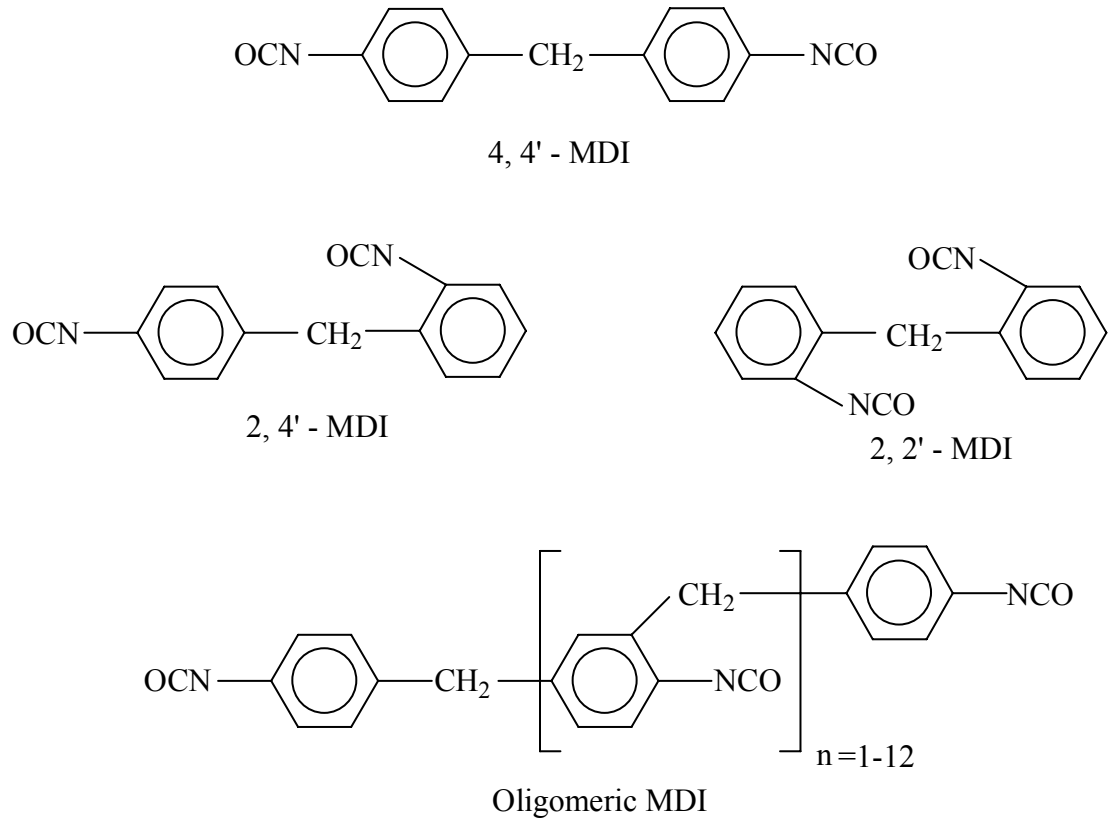

Figure 1.1 – Typical monomeric and oligomeric components of pMDI resins.

OSB is usually produced with a mixture of locally available tree species, including hardwoods and softwoods, which have different physical, chemical, and surface properties. In the southern United States OSB is produced from southern pine grown largely upon plantations. Mixed hardwoods are also used, among these yellow-

poplar is very common. Differences in species mix and harvest site can affect pMDI/wood adhesion.

Early research on pMDI has focused on differences between pMDI and PF performance in composite applications (1-6). As pMDI use grew in composite panel manufacture, pMDI/wood cure chemistry has increasingly been studied (8-14). Species dependent pMDI adhesion has not been extensively studied (13-16). Southern yellow pine (*Pinus sp.*) and yellow-poplar (*Liriodendrum tulipifera*) are two species that are commonly used for OSB manufacture in the Southeastern United States. Understanding differences in pMDI adhesion between these species would be valuable for both academia and industry.

This work is an investigation of the species dependence of pMDI/wood adhesion using southern yellow pine and yellow-poplar. Three complimentary methods of analysis have been utilized:

1. Mode-I fracture testing of adhesion.
2. Wood surface analysis.
3. Synthesis of isotopically labeled pMDI to enable solid-state nuclear magnetic resonance (NMR) analysis of cure with wood.

CHAPTER 2

LITERATURE REVIEW----------

2.1 pMDI/WOOD ADHESION

2.1.1 History

In the 1930's, organic isocyanates were developed in Germany by Bayer Chemical Company for fiber applications (17). Initially, organic isocyanates were used as German aircraft adhesives in World War II (18). In 1954, Goodyear synthesized pMDI by phosgenation of oligomeric amines from the aniline/formaldehyde reaction, but this process was never patented (19). Bayer, ICI and Carwin/Upjohn separately developed industrial processes for the production of 4,4'-MDI, which comes from the distillation of pMDI. Organic isocyanates such as MDI are used in the production of polyurethanes, which are valued for making foams, plastics, films and fibers. Wood adhesion applications amount to a small percentage of the total pMDI market (20).

As early as 1932 Hartman used isocyanates to produce hydrophobically modified cellulose (21). The first wood product manufactured with an isocyanate binder was Phenapan – V – 100 – Iso – Spanplatte by Dusetsche Novopan of West Germany (1). This wood particle product had PF faces and a pMDI core. The first North American composite product using an isocyanate binder was called Elcoboard from Ellingston lumber (1). Elcoboard was the first structural multi-ply panel produced with pMDI, and also the first composite panel to be hot pressed in one step. PMDI was used in the production of waferboard in 1985. Today pMDI is primarily used as an OSB binder. Its advantages over other adhesives include faster press times, higher strength, and higher

durability (1-6). Its other most significant use in the Forest Products industry is for the manufacture of laminated strand lumber.

2.1.2 Isocyanate/Wood – Composite Research

Isocyanate bonded composite materials have been extensively produced and tested in academic and government laboratories. Early research focused on making wood resistant to degradation using aliphatic isocyanates (22). Later, in the late 1960's research was conducted using aromatic isocyanate binders for particleboard (1). Deppe and Ernst reported that pMDI bonded wood panels achieved the V_{100} rating (West German standard) for use as a building material (22). Their work showed pMDI panels to be as strong as PF bonded panels.

One of the first studies of pMDI flakeboard binders in this country was conducted at Purdue University in conjunction with the Forest Products Laboratory (USFPL) and Mobay chemical (8). Utilizing red oak flakes, it was found that pMDI cured faster than PF. Furthermore, the pMDI bonded panels exhibited higher modulus of elasticity (MOE), modulus of rupture (MOR), wet and dry internal bond (IB) and lower thickness swell (TS). Another study conducted at Michigan Technological University showed similar results in mixed-species hardwood and aspen flakeboard (1).

The majority of work first performed on pMDI involved comparisons to PF. Many studies have compared the resins showing pMDI/wood composites to have faster press cycles, higher moisture tolerance and superior physical properties at lower resin loadings and lower press temperatures (2-6). Furthermore, it has been shown that pMDI can tolerate furnish MC's up to 18%, which is much greater than for PF, and could provide significant energy savings (15,23).

2.1.3 pMDI/Wood – Adhesion Mechanisms

In adhesion science, five theoretical adhesive mechanisms are often described. These are the mechanical interlock theory, the diffusion theory, the electronic theory, the adsorption or specific adhesion theory and the theory of covalent bonding (24). It is commonly believed that only three of these mechanisms are potentially important for wood bonding: 1) Mechanical Interlock, 2) Adsorption and 3) Covalent Bonding. Mechanical interlocking occurs when the liquid adhesive flows into wood surface voids and crevices and subsequently hardens, becoming mechanically interlocked with the substrate. Wood porosity strongly promotes mechanical interlocking because adhesives typically penetrate into xylem pores readily. The adsorption theory states that adhesion results from intermolecular interactions between adhesive and substrate. The adsorption theory is thought to be the most important adhesive theory for wood and most other materials. Finally, the theory of covalent bond formation is possible when adhesive and substrate have the chemical functionality to form a primary bond, generally covalent bonds. This adhesive mechanism would be particularly beneficial in terms of bond durability.

2.1.4 pMDI/Wood – Cure Chemistry

Many theories of pMDI/wood bonding have been formed and it is likely that a combination of these occur. pMDI is a 100% organic substance; therefore it has a low surface energy, approximately 45 mJ/m^2, which enables it to easily wet the wood surface (27). Industrial pMDI used in OSB has a low viscosity (~200 cps). Given the low

viscosity and surface energy, it is no surprise that pMDI penetrates rapidly and deeply into wood. PMDI has been shown to penetrate to depths of several millimeters into the wood surface (16, 61).

Because isocyanates react with alcohols to produce urethanes, early researchers believed that urethane linkages formed between wood hydroxyls and isocyanate resins (20, 25). Several have shown that urea linkages and sometimes biuret linkages dominate the pMDI/wood bondline. (9-13, 23, 26). The possible pMDI reactions with wood are shown in Figure 2.1.

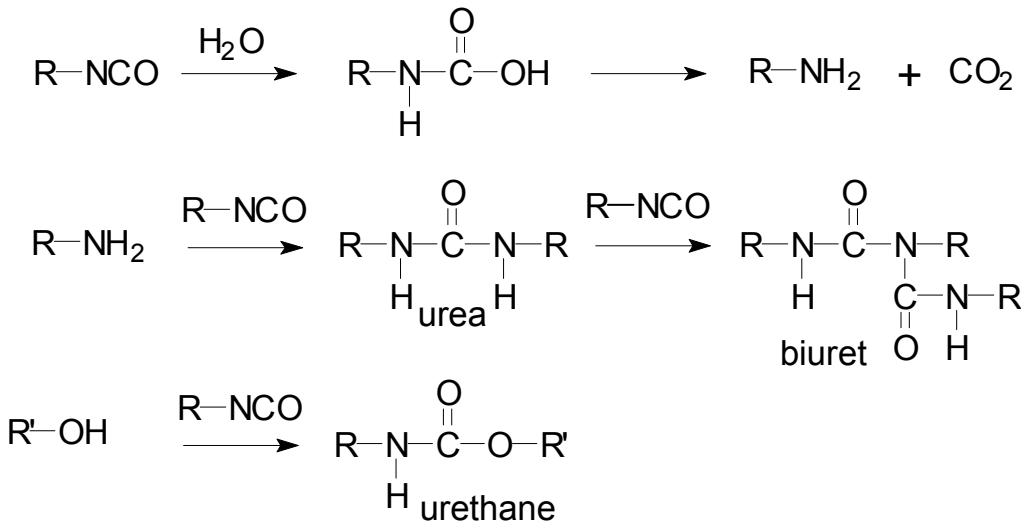

Figure 2.1 Reactions thought to occur in the wood/isocyanate bondline.

As pMDI cures it will most likely react with free and bound water molecules in the vicinity of the wood surface. As seen in Figure 2.1, the isocyanate/water reaction forms carbamic acid that breaks down into an amine and carbon dioxide. These amine functional groups will react rapidly with isocyanate to form a urea network. Consequently, the polymerization of pMDI is dependent upon wood moisture. The urea

can again react with an isocyanate to form biuret. While not shown in Figure 2.1 biuret could further react with isocyanate to form tri-, tetra- or polyurets. Most importantly an isocyanate can react with the hydroxyl group of a wood polymer to form a covalent urethane linkage. The following review discusses some of the different analytical methods used to understand pMDI cure chemistry.

The cure chemistry of isocyanates with wood has been studied extensively with many techniques. Rowell and Ellis showed urethane formation between southern yellow pine and methyl isocyanate using Fourier transform infrared spectroscopy (FTIR) (22). Steiner, Chow and Vadja performed differential scanning calorimetry (DSC) on aspen (*Populus tremuloides*) wood flour and wood flour mixed with pMDI adhesive (28). They showed that pMDI was stable when heated under N_2 gas in the absence of water. It was hypothesized that most resin cure occurred between 110°C to 160°C due to water reaction to form urea bonds. FTIR was performed on white spruce (*Picea glauca*) flakes treated with pMDI; it was shown that temperature and time produce spectral changes that could indicate different stages of urethane or urea formation (28). FTIR studies also indicated that pMDI and lignin react rapidly at room, and at elevated, temperatures. The combination of FTIR and DSC data indicated that pMDI cures in two distinct phases (28).

Owen, Banks and West also studied the wood-isocyanate reaction using FTIR (23). They reacted n-butyl isocyanate with Scots pine *(Pinus sylvestris*) wood, isolated lignin and holocellulose. Their results showed that lignin was more reactive than holocellulose. In another study, again using FTIR, Weaver and Owen studied the isocyanate-wood reaction with phenyl isocyanate, glucose, cellulose, lignin and wood at

various moisture contents (26). FTIR spectra (carbonyl region) of wood reacted with isocyanate above 7% MC strongly resembled products from of the water/isocyanate reaction. It was found that cellulose and lignin both reacted with the isocyanate, but that lignin reacted much faster. The results with industrial pMDI correlated to results with phenyl isocyanate. The reaction products of pMDI with wood at 19%, and also with saturated wood, appeared similar by FTIR; both appeared similar to the water/pMDI reaction products. In all the before mentioned spectra there was no evidence of a direct chemical bond. However the authors believed urethane formation was present with oven dry wood and a large excess of phenyl isocyanate. It was concluded that the nature of the isocyanate reaction with wood is dependent on the moisture content (26).

Wendler and Frazier studied cellulose/isocyanate cure chemistry with ^{15}N labeled pMDI (pMDI-^{15}N) utilizing cross polarization/magic angle spinning (CP/MAS) NMR (8). Cellulose composites of varying moisture content were prepared with a 25% resin loading of pMDI-^{15}N. It was found that the cure chemistry was dominated by biuret-type structures at lower moisture contents. At higher moisture contents, polyurea dominated bondline chemistry. In these cellulose/pMDI composites urethane formation was not detected, however urea and urethane signal overlap may have obscured detection. The labeled pMDI used in this study had an unusually high molecular weight (M_n = 440 g/mole, M_w = 4500 g/mole) compared to industrial pMDI.

Wendler and Frazier examined yellow-poplar/pMDI cure chemistry at selective precure moisture contents (9). It was found that the cure in ovendried wood/pMDI composites was dominated by biuret formation. At 4.5% to 31% precure moisture content it was found that urea linkages dominated bondline cure. Overall it was shown

that urea and biuret dominated wood/pMDI cure and urethane formation was difficult to detect because of signal overlap. Residual isocyanate was detected under all conditions.

Wendler and Frazier further studied pMDI cure chemistry by examining the effects of cure temperature and time (10). Their results showed that as cure temperature increased, network cure changed from polyurea to biuret. A shift from polyurea to urethane dominance was hypothesized at a 60-minute press time at 185° C. The authors stated that urethane formation could result from the breakdown of biuret-type structures. This study used the same high molecular weight pMDI as the previous two studies, which could have influenced the results.

Ni and Frazier repeated much of Wendler and Frazier's work with a much lower molecular weight pMDI, similar to industrial preparations (11, 12). ^{15}N CP/MAS measurements were performed on samples that were pressed at 120° C and 185° C at 500 psi for 20 minutes. They found that urethane might be forming at low temperature and short cure times. At longer press times and higher temperatures, urea dominated the cure chemistry and residual isocyanate decreased. It was suggested that as the cure time increases, cleavage of urethane linkages occurs forming other chemical structures. As in Wendler's research, all press times in this study indicated a dominance of urea. Unlike Wendler's work, no indication of urethane formation occurred at higher press temperature. In summary, Ni and Frazier's results were similar to Wendler and Frazier's. However, Ni and Frazier found evidence for urethane formation. The differences in the respective studies were attributed to the large difference in pMDI molecular weight.

Bao et al. performed solid-state NMR studies of pMDI with aspen and southern pine (13). They investigated the influence of temperature and wood moisture content using ^{15}N labeled pMDI adhesives. Composites were made by applying 10% by weight pMDI resin to veneers with precure moisture contents of 7% or 14%. ^{13}C spectra gave little information due to signal overlap. ^{15}N spectra of pMDI bonded to dry cellulose and REPAP lignin gave an indication of urea, biuret and possibly some urethane formation. The reaction of pMDI with aspen (7%MC) was similar to the reaction of pMDI and water. They concluded that the rate of reaction as a function of temperature and moisture content seems to be greater in southern pine compared to aspen. This was the first demonstration of a wood species effect on pMDI cure.

Marcinko et al. explored the physicochemical nature of pMDI/wood adhesion (14). They used ^{13}C solid state NMR and dynamic mechanical analysis (DMA) to probe molecular motions in aspen, with and without the presence of pMDI. It was shown that cured pMDI changes the physical nature of wood on the molecular scale. Solid-state NMR results indicated a decrease in the molecular mobility for lignin and hemicellulose in the presence of pMDI.

2.1.5 Species Dependent Performance of pMDI Adhesion

Johns et al. investigated the species dependence of pMDI binder performance in flakeboard using five wood species: Douglas-fir, white fir, red oak, hickory and loblolly pine (15). Some variability between species occurred in processing; this included slight differences in panel density, face and core flake thickness and the face: core: face weight

ratio. A species effect was shown for internal bond (IB), modulus of rupture (MOR), modulus of elasticity (MOE), wet MOR and linear expansion (LE) measurements. Panels from southern pine consistently performed worse than panels made from all other species. It was concluded that precure moisture content and wood species were the major causes of differences in panel performance.

Phanopoulous et al. identified a species dependence with pMDI using Scots pine and aspen (16). Differences in resin penetration and static contact angle were shown. These results were compared to thickness swell (TS) and IB from OSB boards bonded with 6% resin. They found pMDI wetting and penetration with aspen was better than with Scots pine. This correlated to slightly better internal bond and thickness swell results.

As the literature has shown, pMDI adhesive performance with wood is dependent on many variables. Some of these include wood species, wood moisture content, bonding conditions (pressure, temperature, rate, etc.) and particle geometry (planer shavings, flakes, fibers, etc.). To date, only three references have specifically investigated species dependent adhesion. Bao et al. showed that aspen and southern yellow pine bonded with pMDI gave slight differences in cure chemistry. Johns et al. demonstrated that similarly prepared flakes of different species performed differently in flakeboard composites. Lastly, Phanopoulous et al. showed species dependent OSB properties that correlated with better wetting and penetration in aspen vs. Scots pine. These works indicate that pMDI performance is species dependent.

The goal of this work was to further advance our understanding of pMDI/wood adhesion and its wood species dependence. Two species, yellow-poplar and southern

pine, were selected for this investigation. Methods of analysis include mode-I fracture cleavage, surface energy analysis and synthesis of labeled pMDI to support a solid-state NMR analysis. The solid-state NMR analysis using the labeled pMDI is not a part of this work.

2.2 A GENERAL COMPARISON OF SOUTHERN YELLOW PINE AND YELLOW-POPLAR

2.2.1 General Characteristics

The species that comprise the southern yellow pines include Longleaf pine (*Pinus palustris. Mill.*), Shortleaf pine (*Pinus echinata*), Loblolly pine (*Pinus taeda*), Slash pine (*Pinus elliotti Engelm.*), Pitch pine (*Pinus rigida Mill.*), Pond pine (*Pinus serotina Michx.*), Spruce Pine (*Pinus glabra Walt.*), South Florida slash pine (*Pinus elliottii var. densa Little and Dorman*), Table Mountain pine (*Pinus pungens Lamb.*) and Virginia pine (*Pinus virginiana Mill.*). The four principal species that make up 90% of the total inventory of the southern pines in the commercial forest are longleaf, loblolly, slash and shortleaf (29). The wood is straight to uneven-grained with medium texture, an average green specific gravity of 0.45-0.59, and 0.52-0.66 oven-dry. Transverse resin canals may have diameters up to 70 microns and longitudinal tracheids can be up to 60 microns in diameter, but average 35-45 microns. These species cannot be separated on the basis of wood structure and are usually marketed according to density (29).

Yellow-poplar (*Liriodendrum tulipifera L.*) is a single species and is also referred to as tulip poplar or whitewood. It grows mainly in the south, but its range spans as far north as Michigan, Ontario and New England. The wood is straight-grained, with

specific gravity approximately 0.38 green, and 0.43 oven-dry. Yellow-poplar is a diffuse porous hardwood. On average there are 4-7 rays per mm and fiber tracheids are about 6-15 microns in diameter (30).

2.2.2 Anatomy

The ten species referred to as the southern pines are so anatomically similar that they cannot be differentiated by classical methods. There is an abrupt transition between earlywood and latewood. Annual rings are approximately $1/16^{th}$ to 1 inch in thickness. Most southern pines are harvested below 50 years of age and trees of this age consist mostly of sapwood. Longitudinal tracheids make up over 90% of the volume of southern pine wood. Other longitudinal cell types in southern pine include strand tracheids, epithelial cells and longitudinal parenchyma. Horizontal cell types include ray tracheids, ray parenchyma and epithelial cells. Most rays in southern pines are uniseriate. Exceptions include fusiform rays, which contain horizontal resin canals. Six types of pit pairs occur in southern pines – tracheid to tracheid (bordered), tracheid to ray tracheid (bordered), ray tracheid to ray tracheid (bordered), tracheid to ray parenchyma (half-bordered), ray tracheid to ray parenchyma (half-bordered) and ray parenchyma to ray parenchyma (simple). Most pitting occurs on the radial face of the longitudinal tracheids with some on the tangential face. Tracheid length, fibril angle and transverse measurements all vary slightly within species and between the southern pines (29).

Yellow-poplar vessels are numerous and in radial multiples that can and often are diagonal. The vessel distribution is variable, and is less numerous in the latewood compared to the earlywood. Yellow-poplar like all other hardwood species consists of

many cell types. Longitudinal cells include vessel elements, fibers (fiber tracheids and libriform fibers), axial parenchyma (strand, fusiform and epithelial). Horizontal cells only consist of ray parenchyma and there are two types – procumbent cells and upright cells. The fiber tracheids contain bordered pits and the libriform fibers have simple pitting. Longitudinal axial parenchyma cells have simple pitting, short lengths and serve as living storage reservoirs in the sapwood of the tree. Yellow-poplar contains heterocellular rays composed of both procumbent and upright cells. Multiceriate rays in yellow-poplar usually only contain a single row of upright cells at the top and bottom of the ray (tangential view). Proportions of cell types in yellow-poplar stemwood are 43.3% vessels, 42.6% fibers, 11.4% rays and 2.7% parenchyma of trees sampled from 22 southern yellow pine sights. Five types of pitting occur in hardwoods like yellow-poplar. Differences in pitting, especially on the radial and tangential faces between southern pine and yellow-poplar should greatly influence the ability of resin penetration (31).

2.2.3 Chemistry

All wood is made of cellulose, hemicellulose, lignin, extractives and inorganic components. Southern pine is made up of approximately 43(+/-2)% cellulose, 24(+/-3)% hemicellulose (9(+/-2)% of those xylans and small amounts of arabinogalactan and pectin), 25% to 30% lignin, 3% to 9% percent extractives and <1% inorganics (29). Yellow-poplar is composed of 39.1% cellulose, 28% hemicellulose, 30.3% lignin, 2.4% extractives and 0.3% ash (32). Lignin in gymnosperms, such as pine, is mainly comprised

of guaiacyl lignin structures. In angiosperms such as poplar, lignin has a combination of syringyl and guaiacyl structures (33).

Isocyanates are reactive with chemical groups that contain active hydrogen; this includes: alcohols, phenols, carboxylic acids and water. Consequently, all structural polymers in all woods could form primary bonds with isocyanates. Southern pine and yellow-poplar contain extractives that could interfere with the adhesion process. Three predominant extractive types are short chain carbohydrates, phenolics and resins. Carbohydrates include sugars, cyclitols, and polysaccharidic substances such as gums, mucilages, starch, pectin and galactans. These extractive chemicals are soluble in water (34). Phenolic extractives include: hydrolyzable tannins, flavonoids, lignans, stilbenes and tropolones. These extractives are mainly found in bark and heartwood and are acetone soluble (32). Resins include terpenes, resin acids, fatty acids and esters, various alcohols, hydrocarbons and other neutral compounds soluble in nuetral, non-polar organic solvents (35). Table 2 lists the approximate percent of these types of extractives in each species.

Table 2.1 - Percent wood extractives in southern yellow pine and yellow-poplar (35).

Species	Carbohydrates	Phenolics	Resin
Yellow-poplar	2.0	1.0	0.2
Southern Pine	3.0	4.0	3.3

It can be seen in Table 2.1 that pine contains a higher percentage of extractives than yellow-poplar. Many of these extractive compounds contain hydroxyl and carboxylic acid groups that are capable of reacting with isocyanate and interfering with

adhesion to wood polymers. Because of the higher percentage in pine it could be hypothesized that the extractive interference would be greater than in poplar.

Also, these extractives could interfere with the resin's ability to penetrate the bulk wood. It is known that as the wood surface ages its surface free energy decreases because of extractives migration. A higher amount of extractives in pine may correlate to high amounts of extractives in the pine surface. If this is the case, it would retard pMDI wetting.

In summary, southern yellow pine and yellow-poplar have many different chemical and physical properties that could affect pMDI adhesion. Physically, pine and poplar have large differences in anatomy, density and EW/LW transitions. Both species have similar chemical components that could react with pMDI, but these occur in different proportions. The major differences between pine and poplar is that pine has approximately twice the amount of extractives - poplar has a larger percent of hemicelluloses. These physical and chemical differences could influence the quality of pMDI adhesion.

This research investigates the species dependence of pMDI/wood adhesion. Three complimentary methods have been used:

1) Mode-I fracture testing of adhesion.
2) Wood surface analysis.
3) Synthesis of isotopically labeled pMDI to enable solid-state NMR analysis of resin cure.

CHAPTER 3

SPECIES DEPENDENCE OF pMDI ADHESION IN FRACTURE CLEAVAGE TESTING----------

3.1 INTRODUCTION

In the past thirty years fracture cleavage testing has been used to quantify the strain energy release rate (fracture toughness) of adhesives bonded to different substrates. This methodology has been applied to wood starting with the work of Ebewele et al. (37). Many researchers have investigated the effects of specimen geometry, wood species, and adhesive type (38-42). Recently, Gagliano and Frazier have simplified the procedure for testing and data analysis (43).

This study examines pMDI adhesion using mode I fracture cleavage. The main goal was to examine the species effect of pMDI adhesion. Because of their commercial importance, yellow-poplar and southern yellow pine were chosen for this study using two different industrial pMDI adhesives. Secondly, the effect of plastic loss in the flat double cantilever beam (DCB) was examined. Lastly, durability of pMDI adhesion for both species was examined with mode I fracture cleavage.

3.2.1 LITERATURE REVIEW

3.1.1 Theory

In 1920, A.A. Griffith developed the theory of crack propagation to describe the phenomenon of brittle fracture in solid materials. Two conditions must be met for a crack to propagate through a material; first it must be energetically desirable (during crack propagation the energy stored in the material is being reduced) and secondly there

must be a molecular mechanism for energy transformation (44). During propagation, regions of the fracture surface release their stored energy (strain energy), which can be quantified as the strain energy release rate. Griffith proposed a critical crack length l_g, which causes catastrophic propagation. Past this point a crack will produce more energy than it consumes and destructive failure will occur. In order to produce a new fracture surface the chemical bonds at the fracture surface must be broken. Once fracture occurs the molecular structure of the material will be damaged. Thermosetting polymers, such as pMDI are known for relatively low fracture energy ~ 100 J/m^2 and behave like a glass. Thermoplastics, which are rarely used in wood composites, have approximately 100 times the work of fracture of thermosetting adhesives (44).

The use of fracture mechanics allows us to investigate two types of material parameters. The first parameter described is the stress field at the crack tip and the second parameter is the fracture toughness. Fracture mechanics testing can be performed in three modes: I, II, and III. Mode-I is opening cleavage: Mode-II is shear and Mode-III is tearing.

Ripling and Mostovoy were the first to test adhesive bonds by investigating fracture toughness in adhesive systems. They used a tapered dual cantilever beam (TDCB) adhesive specimen and showed that Mode-I fracture toughness testing was a viable method (45).

3.2.1 Fracture Mechanics of Adhesives Bonded to Wood

Wood adhesives are tested in many ways. The most common is probably the shear block method according to ASTM D 905 (46). Disadvantages of this method include the reliance on wood failure (not adhesive failure) and subjective determinations of wood failure. Internal bond testing (tension perpendicular to surface, ASTM D1037) is used for evaluating adhesively bonded wood composite panels. The disadvantage of this method is that other contributions such as flake geometry and panel density affect IB results. Fracture mechanics can more effectively evaluate the adhesive bondline. This is because the adhesive and adhesive interphase is cleaved without macroscopic wood failure.

Ebewele, River and Koutsky were the first to apply the mode I fracture test to wood adhesives using a TDCB (tapered double cantilever beam) specimen (37). They summarized some key problems with testing bonded wood in tension or shear: stress concentrations from specimen geometry, sample specific stress distributions, failures initiated by complex and unknown stress modes, wood failure, and the related need for many test replications. In their experiment they used the TDCB geometry and evaluated bondline thickness and grain angle effects using hard maple bonded with a phenol-resorcinol-formaldehyde adhesive. They found that from a bondline thickness range of 70 to 160 microns, 90 microns was optimal. Secondly, it was recorded that grain angle had a pronounced effect on fracture energy (G_{IC}) in specimens tested in a range from 0 to 90°. The lowest values for G_{IC} occurred at a 20° grain angle. The highest occurred at a 90° grain angle in a range of samples from 5° to 90°.

River and Okkonen examined wood adhesives using a composite contoured double cantilever beam (CDCB) method (39). They constructed their tapered beam from oriented strand board (OSB) instead of aluminum, which was used in all previous studies. According to the authors, disadvantages of using the aluminum/wood backings included: 1) only 40 to 50mm of the bondline can be used for calculating G_{IC}; 2) the contoured aluminum beams are expensive and 3) chemical etching needs to be performed for every new sample made. In their study, the OSB backings gave reliable results and could be reused more simply than the aluminum beams.

Lim et al. investigated G_{IC}, G_{IIC}, and G_{IIIC} using the DCB (double cantilever beam) specimen geometry (41). They found a correlation between G_{IC} and tensile strength, but did not find a significant correlation between G_{IIC} and shear strength. It was concluded that $G_{IC}<G_{IIC}<G_{IIIC}$, using the compliance method of beam theory.

Schmidt evaluated PF and pMDI adhesives using a DCB specimen geometry (42). The research investigated bonded wood specimens with simple beam theory, corrected beam theory and the compliance method of beam theory. It was found for a high molecular weight PF resin that the compliance method of beam theory gave results with lower standard deviation with crack lengths from 40mm to 110mm. In this experiment, pMDI bonded DCB specimens had a higher fracture toughness value than PF bonded specimens. Weathered PF bonded specimens had higher fracture toughness than non-weathered specimens. Non-weathered pMDI bonded specimens had higher fracture toughness than weathered specimens.

Gagliano and Frazier investigated two different methods of data analysis on flat DCB specimens bonded with a PF impregnated paper (43). It was shown that the shear

corrected compliance method from beam theory gave more reliable results than the direct compliance method. This enabled a simpler composite geometry and further reduced specimen preparation time.

The following analyzes the wood species dependence of pMDI adhesion with fracture cleavage testing utilizing the simple flat DCB specimen geometry employed by Gagliano and Frazier. In conjunction with examining the wood species dependence of adhesion, the effects of plastic loss with the wooden DCB geometry were investigated. Wood species effect on pMDI adhesive durability was also examined.

3.3 SAMPLE PREPARATION

12' x 1' x 2" (30.48 cm x 2.52 cm x 5.04 cm) boards of each species were cut into one foot sections (billets). A billet (see figure below) was cut into0.59" (15 mm) thick laminae with a 5° grain angle on a 1" band saw (3.1). Each lamina was conditioned to 10% EMC in an environmental chamber. Conditioned laminae were planed immediately prior to bonding to expose a fresh bonding surface and attain the final thickness of 10mm (0.39"). Bonding surfaces were coated with pMDI adhesive using a wire-wound metering bar. Typical adhesive coverage was approximately 80 to 120 g/m^2. Bonding surfaces presented radial and tangential planes, the relative degree depending upon the parent billet. These laminae were then sandwiched together and pressed at 175°C and 0.55MPa for 20 minutes. Two separate adhesives were used: Huntsman Rubinate 1840 and Bayer Mondur 580. These are both commercially available industrial OSB core resins. Later, the Huntsman and Bayer resins will be referred to as pMDI-A and pMDI-B respectively.

Microdielectric analysis was performed on two laminae each of pine and poplar to monitor cure. Measurements were made with a Micromet Eumetrics III dielectric analyzer. A type K thermocouple and a Micromet IDEX sensor were placed in the bondline of each laminate. Dielectric analysis frequencies were 1, 10, 100, 1k and 100kHz.

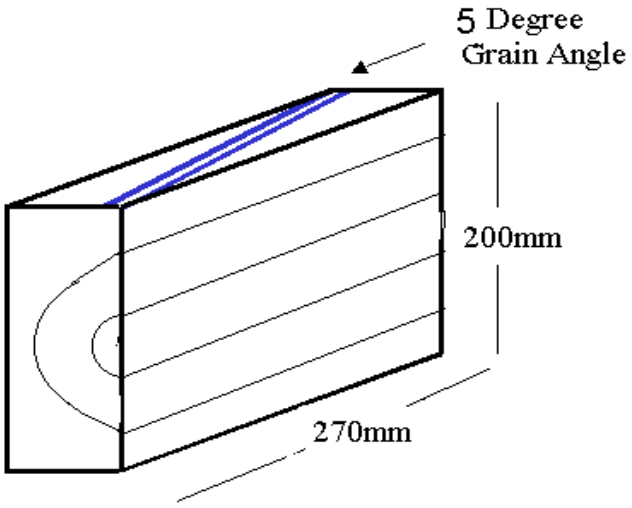

Figure 3.1 – Representation of laminae being cut out of a billet of wood.

The bonded laminates were reconditioned to 10% EMC and then ripped into specimens 20mm wide by 200mm in length for fracture testing (Figure 3.2). One laminate yielded 5 to 6 specimens.

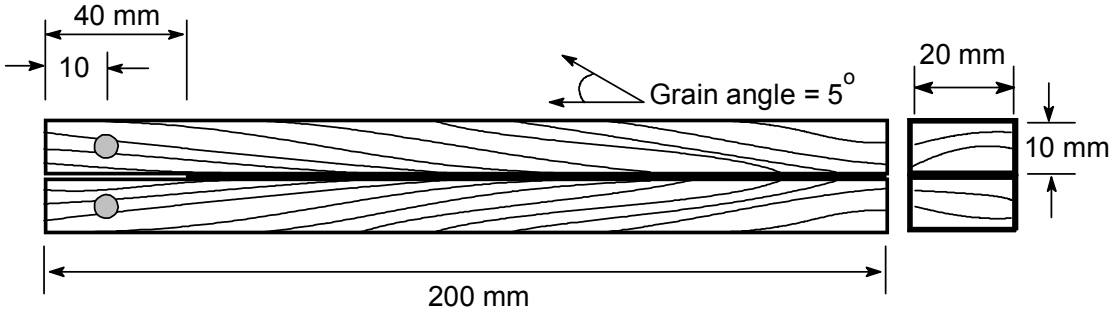

Figure 3.2 – Mode-I double cantilever beam fracture toughness specimen

3.4 TEST PROCEDURE

Fracture analysis was performed in Mode-I cleavage with the double cantilever beam specimens described above. The cross-head displacement rate for sample cleavage was constant at 2 mm/min. Crack lengths were measured with a 10x magnification CCD video camera, which was secured to a traveling stage. Each DCB sample was pulled open in Mode-I cleavage. When bondline fracture initiated, the crosshead was stopped and held motionless for 12 seconds. Within 12 seconds, crack arrest occurred and the arrest crack length was measured. The crosshead was then returned back to zero displacement and the process was repeated cyclically until catastrophic failure. Ten to twenty cycles were obtained per sample as shown in the raw data plot of load vs. displacement, Figure 3.3 below.

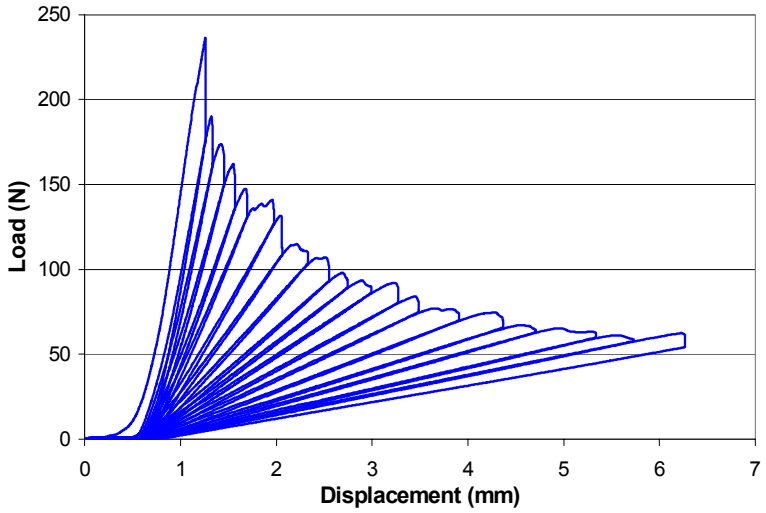

Figure 3.3 – Typical Load vs. Displacement Raw Data for Mode-I Fracture Testing

Analysis of the data was performed utilizing the shear corrected beam theory via the compliance method (43). The general relationship between fracture energy and compliance according to beam theory is given below (38).

$$G_{IC} = \frac{P^2}{2B}\left(\frac{dC}{da}\right)$$

G_{IC} is the fracture toughness; P is the critical load at crack initiation or arrest; B is the sample width; C is compliance; and a is the crack length. The results were calculated with the DCB specimen in load control. The following shear corrected beam theory equation was used (47).

$$G_{IC} = \frac{P^2(a+x)^2}{B(EI_{eff})}$$

In this equation, x is the crack length offset and EI_{eff} is the effective flexural rigidity of the DCB specimen (47). These values are obtained by plotting the cube root of the compliance vs. crack length as shown in Figure 3.4. Compliance is the reciprocal of the loading curves, like those shown in Figure 3.3. The quantity x is called a 'shear correction factor' (x-intercept), which is used in cases where the adherends have low shear modulus. Beam theory assumes linear elasticity. Because wood is a viscoelastic material the assumption could be flawed.

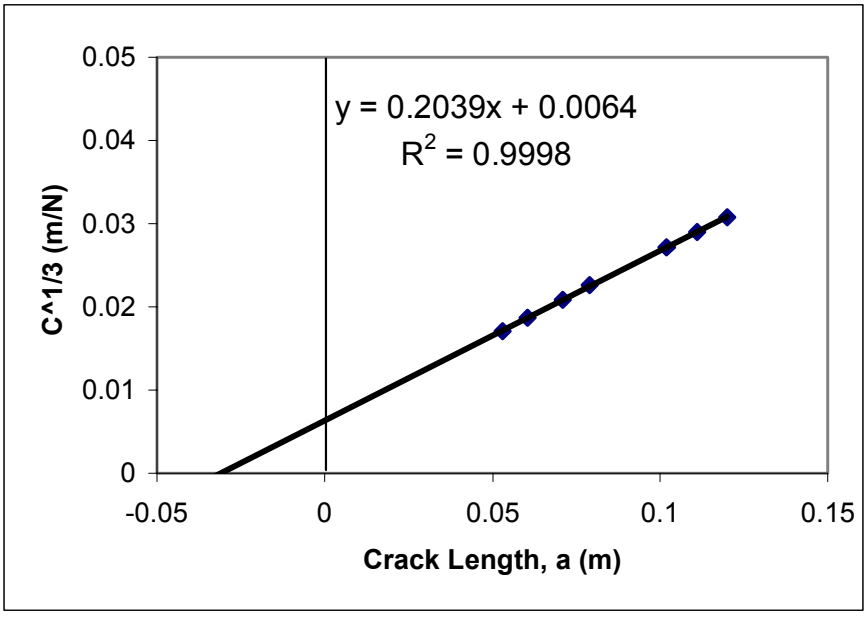

Figure 3.4 – Typical plot of cubed root of compliance vs. crack length obtained for a single fracture specimen

- Specimen Geometry

To analyze the plastic loss in flat DCB specimens, laminae of pine and poplar were stiffened with either ¾" or ¼" plywood backings. Backings were bonded to both sides of laminae with an epoxy adhesive. The backings were cold pressed at 16.5 psi for ten minutes. Specimens were conditioned to 10% EMC before mode I fracture testing.

- Specimen Conditioning

Some specimens were submitted to weathering before test evaluation. Specimens were cut from laminates that were weathered in a 2-cycle test. The edges of each laminate were sealed with silicone caulking before the weathering test was initiated. Each laminate was water soaked for 48 hours, then dried to 5% EMC at 47°C dry bulb, 25°C wet bulb temperature. This two-cycle weathering was repeated twice. Laminates were reconditioned to 10% EMC, then cut into specimens and evaluated.

3.5 RESULTS AND DISCUSSION

3.5.1 Dielectric Analysis

Dielectric analysis was performed during the hot pressing of selected laminates. Representative cure temperature and ion viscosity are shown Figure 3.5 and 3.6. Ion viscosity is the reciprocal of conductivity. Both dielectric plots show a rapid rise in temperature in the first four minutes. For both species, ion viscosity decreases from temperature effects, then finally rises and plateaus. These plateaus indicate that adhesive vitrification was accomplished in both samples, and therefore in all fracture specimens.

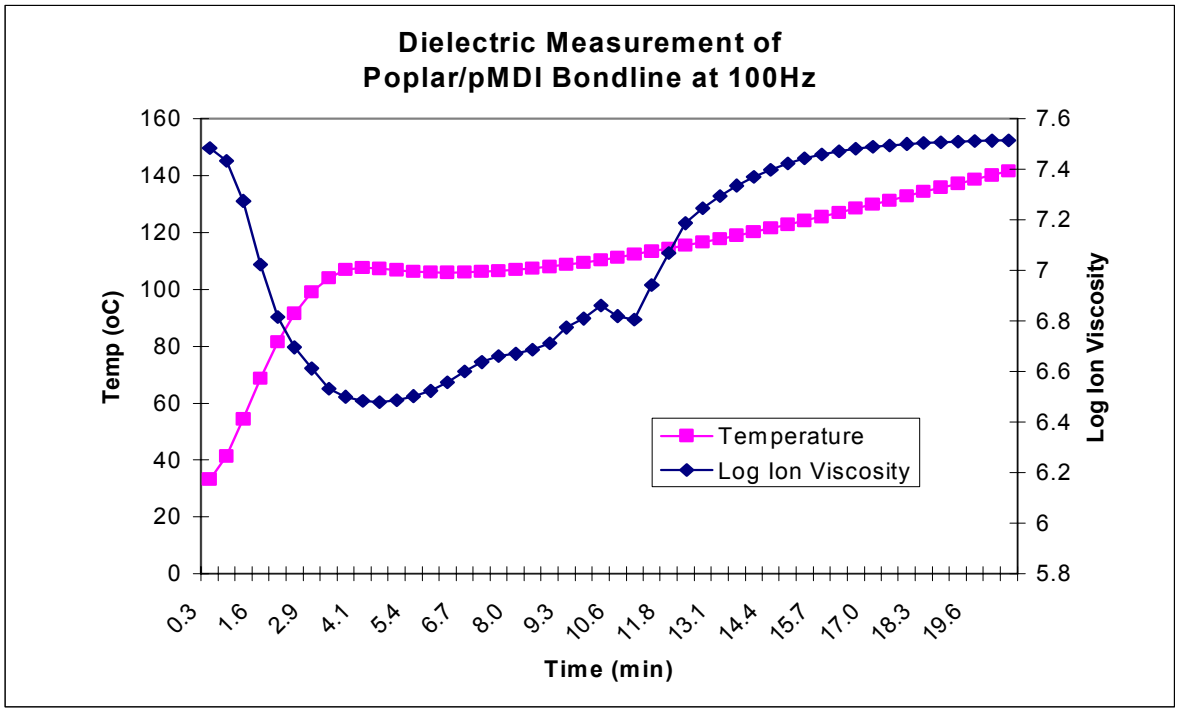

Figure 3.5 – Dielectric analysis of poplar/pMDI bondline

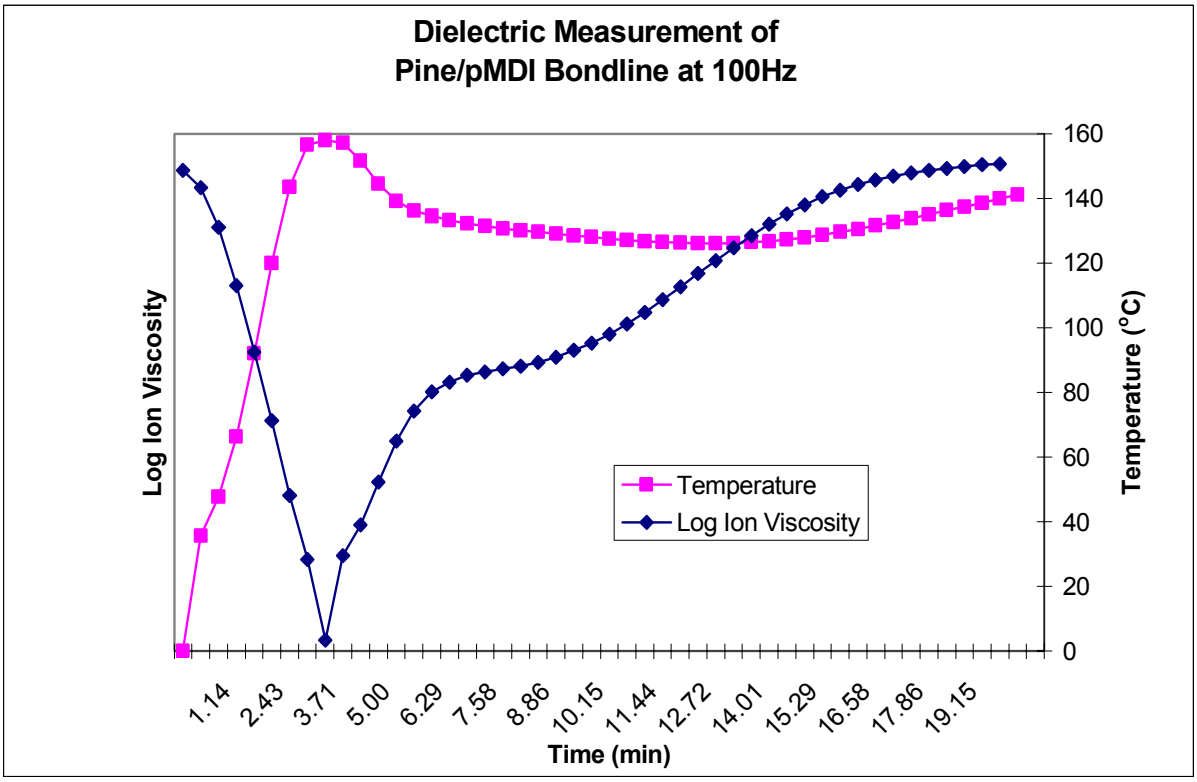

Figure 3.6 – Dielectric analysis of pine/pMDI bondline

Fracture Results – pMDI-A

3.5.2 Species Effect

Specimens of southern yellow pine and yellow-poplar were examined in accordance with the method described above to investigate the species effect of pMDI adhesion. Two pMDI adhesives (hereafter referred to as pMDI-A and B) were used to evaluate pMDI species performance. Both pMDI-A and B are OSB core resins from different manufacturers, but are generally very similar. Two laminates of each species were prepared with pMDI-A and ¼" softwood plywood backings. Table 3.1 lists the results with adhesive A.

Table 3.1 – Species effect of adhesion with pMDI-A (1/4" backing)

Species	Initiation Energy (J/m^2)	Arrest Energy (J/m^2)	Number of Specimens	Number of Cycles	Adhesive Coverage (g/m^2)
Yellow-poplar	129.1 (34.9)*	115.5 (34.1)	10	90	81 119
Southern yellow pine	215.6 (47.3)	200.4 (48.1)	10	66	106 93

*The standard deviation is listed in parenthesis.

The results show a significant difference between pMDI bonded with poplar and pMDI bonded with southern yellow pine. The statistical significance was tested in both cases utilizing a one-sided t-test assuming equal variance at $\alpha = 0.05$ confidence levels. Statistics were based on pooling all cycles from the ten specimens from each species. The results demonstrate that wood species has an impact on the pMDI performance. This is shown for both the initiation (p=1.8E-04) and arrest (p=0.003) fracture energies. Figure 3.7 illustrates the species effect with both species.

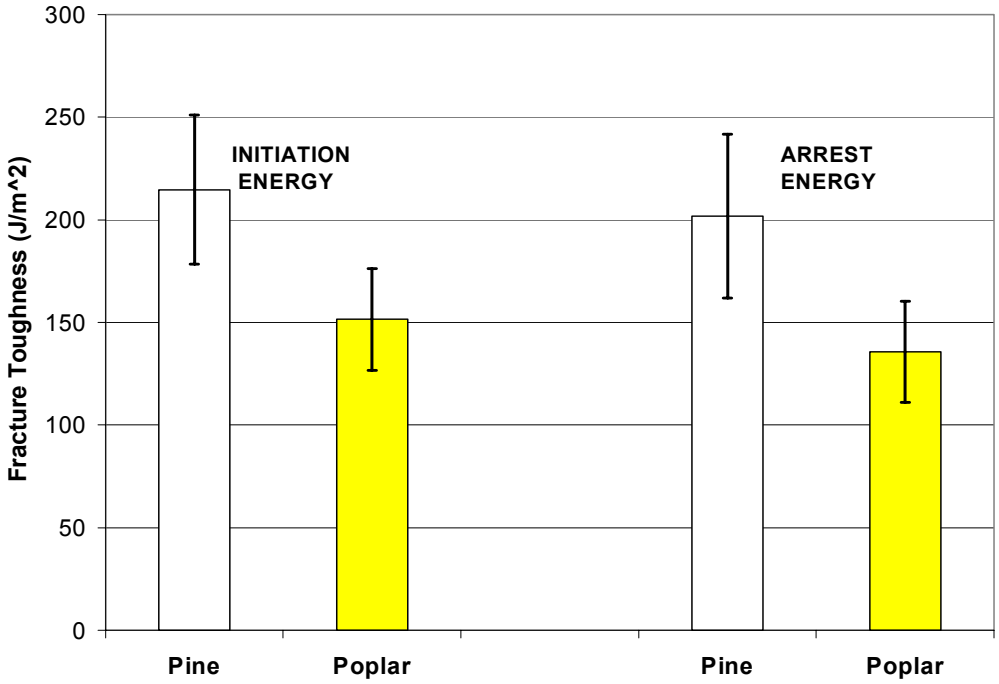

Figure 3.7 – Species effect on initiation and arrest energies for pMDI-A (1/4"backing).

- Species Effect: pMDI-B

The species dependence of pMDI adhesion was also studied using pMDI-B. Three laminates of yellow-poplar and two laminates of southern yellow pine were bonded in the same fashion as mentioned previously. However, in this case a ¾" backing was bonded to the laminates with epoxy adhesive to ensure linear elasticity of the fracture cleavage specimens. Table 3.2 gives the results of the species comparison with the B adhesive.

Table 3.2 – Species effect of adhesion with pMDI-B (3/4" backing)

Species	Initiation Energy (J/m^2)	Arrest Energy (J/m^2)	Number of Specimens	Number of Cycles	Adhesive Coverage (g/m^2)
Yellow-poplar	133.5 (36.3)*	102.0 (30.4)	12	94	136 130 148
Southern yellow pine	242.6 (59.4)	181.8 (55.3)	9	57	114 93

* Standard deviation is located in the parenthesis

A one-sided t-test assuming equal variance (α=0.05) was performed. The cycles from all specimens were pooled together for the statistical test. Pine had significantly higher fracture energies for both initiation (p = 1.5E-07) and arrest (p =1.7E-06), which was the same finding shown previously with pMDI-A.

Fracture cleavage testing demonstrates that pMDI bondline performance is species dependent and that pine exhibits superior performance. Gagliano and Frazier have demonstrated that the fracture method employed here provides results that are independent of variations in bulk wood modulus (43). Consequently, the species dependence shown here is not affected by the modulus difference between poplar and pine. Instead, the species dependence shown here must have another origin such as: wood surface chemistry, wood anatomy, cure chemistry, or a combination of these effects.

3.5.2 Effect of Sample Stiffening on Fracture Toughness

Beam theory assumes linear elasticity of the adherends in a DCB specimen (adherends should exhibit no plastic loss during testing). This assumption was tested by comparing results from simple DCB specimens (Figure 3.2) to DCB specimens stiffened with plywood backings. Two laminates were prepared and stiffened with ¼" softwood plywood backings and two laminates were not stiffened. All laminates in this study were bonded with pMDI-A.

Poplar specimens without stiffening had significantly higher fracture toughness values than those that were stiffened (Table 3.3). Statistical significance was tested with a one-sided t-test ($\alpha = 0.05$). For initiation the p-value was 5.1E-07 and for arrest 3.5E-06, indicating a highly significant effect of sample stiffening. This suggests that plastic loss may occur in the adherends that were not stiffened. Permanent set was not observed in the unbacked specimens, suggesting that plastic loss could be occurring on the micro or molecular level.

Table 3.3 – Poplar backed vs. unbacked ¼" fracture cleavage specimens

Yellow-Poplar	Initiation Energy (J/m^2)	Arrest Energy (J/m^2)	Number of Specimens	Number of Cycles	Adhesive Coverage (g/m^2)
Unbacked	151.5 (24.7)*	135.7 (24.5)	8	102	98 165
Backed	129.1 (34.9)	115.5 (34.1)	10	90	81 119

* Standard deviation is located in the parenthesis

Stiffened southern yellow pine specimens were identical to those without stiffening, Table 3.4. This indicates that plasticity is not a concern with the pine

specimens. More testing is needed to quantify plastic loss in poplar DCB's. Figure 3.8 gives an illustration of the initiation energies between ¼" stiffened specimens and specimens that were not stiffened. Note that Figure 3.8 also demonstrates the species dependence of pMDI adhesion as was shown previously.

Table 3.4 – Pine backed vs. unbacked ¼" fracture cleavage specimens.

Southern Yellow Pine	Initiation Energy (J/m^2)	Arrest Energy (J/m^2)	Number of Specimens	Number of Cycles	Adhesive Coverage (g/m^2)
Unbacked	215.6 (36.3)*	202.4 (39.8)	8	65	92 100
Backed	215.6 (47.3)	200.4 (48.1)	10	66	106 93

* Standard deviation is located in the parenthesis

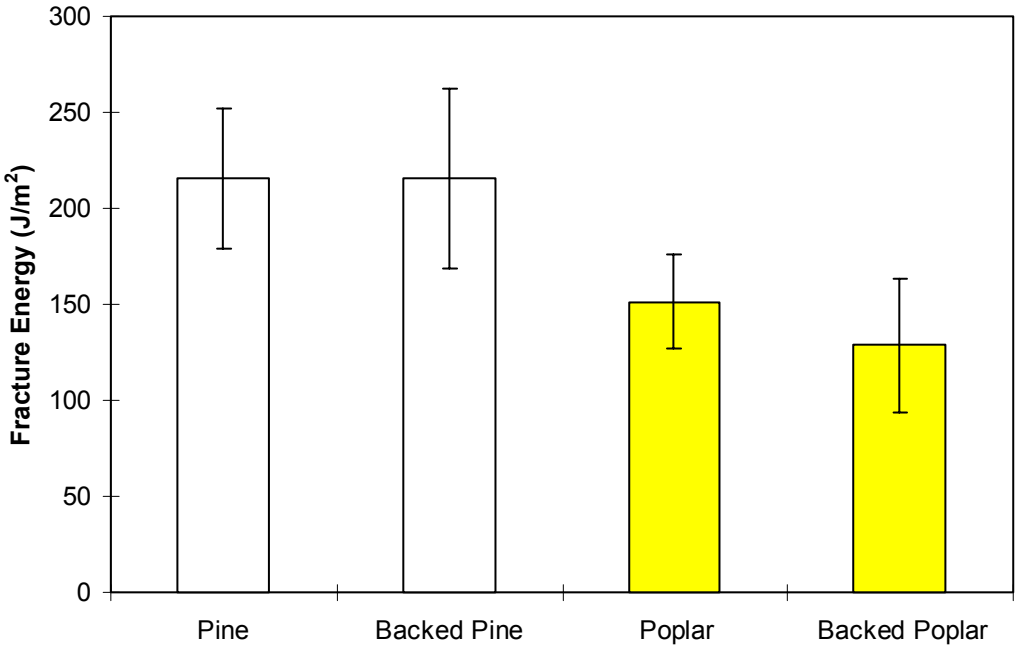

Figure 3.8 – Effects of stiffening on initiation energies in poplar and pine with pMDI-A

3.5.3 Effect of Weathering on Fracture Toughness

Laminates of pine and poplar bonded with pMDI-A were subjected to cyclic weathering to investigate durability. The weathering consisted of a two-day water soak at 1atm followed by conditioning at 47°C dry bulb temperature 25°C wet bulb temperature (5% EMC) for nine days. Laminates were subjected to two cycles of this weathering scheme. Laminate edges were sealed with silicone caulking. Table 3.5 gives the results from unbacked yellow-poplar specimens tested with and without weathering. Table 3.6 gives the results for southern yellow pine. Figure 3.9 plots the initiation energy of the weathered samples vs. the initiation energy of non-weathered.

Table 3.5 – Weathering effect on pMDI adhesion for unbacked poplar

Yellow-Poplar	Initiation Energy (J/m^2)	Arrest Energy (J/m^2)	Number of Specimens	Number of Cycles	Adhesive Coverage (g/m^2)
Weathered	139.12 (56.08)*	127.13 (54.29)	10	78	97 94
Unweathered	151.5 (24.7)	135.7 (24.5)	8	102	98 165

* Standard deviation is located in the parenthesis

Table 3.6 - Weathering effect on pMDI adhesion for unbacked pine

Southern Yellow Pine	Initiation Energy (J/m^2)	Arrest Energy (J/m^2)	Number of Specimens	Number of Cycles	Adhesive Coverage (g/m^2)
Weathered	246.99 (47.87)*	229.56 (52.51)	6	41	101 113
Unweathered	215.6 (36.3)	202.4 (39.8)	8	65	92 100

* Standard deviation is located in the parenthesis

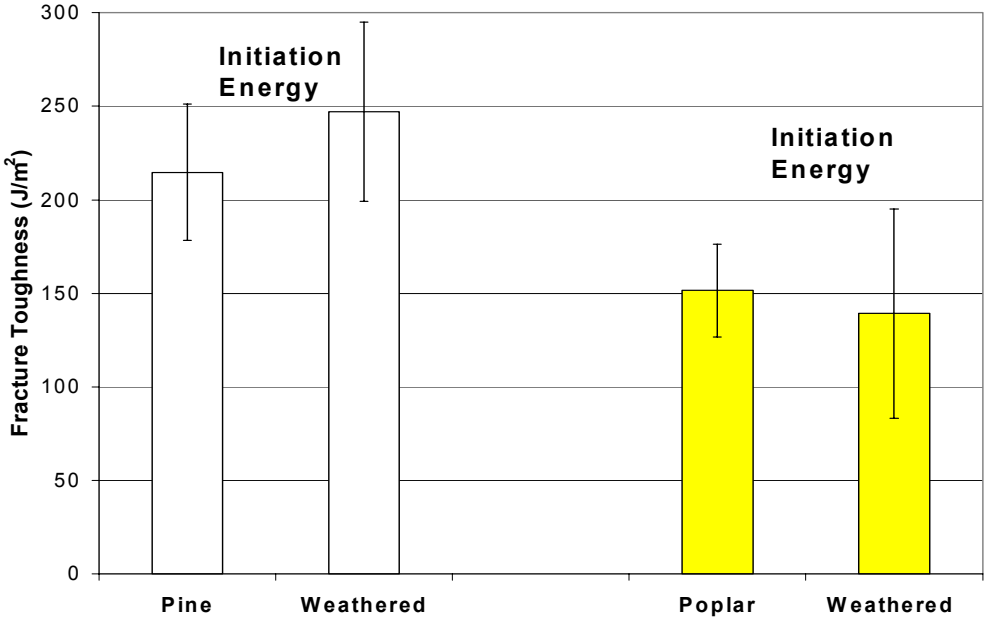

Figure 3.9 – Effects of weathering on fracture toughness

Weathered pine had significantly higher fracture energies than unweathered pine ($p=1.78E-04$). The reason for this is currently unknown although this result has occurred previously with PF bonded DCB specimens subjected to weathering by Schmidt (42). Weathered poplar was significantly lower than non-weathered specimens for initiation energies ($p=0.02$) and arrest energies ($p=0.048$). This indicates that the poplar bondline was adversely affected by weathering. So, not only does the pine show better adhesion than the poplar, but the pine bondlines are also more durable than the poplar bondlines, according to these results.

3.6 CONCLUSION

PMDI bonded pine had a significantly higher fracture cleavage energy (G_{IC} and G_{IA}) compared to pMDI bonded yellow-poplar. The species effect was significant using two different industrial adhesives. All fracture surfaces exhibited no wood failure. This means that each species affected the adhesive bondline differently. The difference in performance could be due to differences in wood structure, surface energy, cure chemistry or more likely a combination of all three.

This research has also shown that the flat double cantilever beam specimen geometry can effectively be used with 10mm thick adherends without stiffening in southern yellow pine. There was no significant difference between stiffened and non-stiffened specimens in pine. There was a significant difference between stiffened and non-stiffened specimens of poplar. No macroscopic plastic deformation could be observed in poplar specimens. Further testing is needed to quantify this effect.

Cyclic weathering was performed on specimens from both species with pMDI-A. Pine showed a significant increase in G_{IC} and G_{IA} after weathering. This phenomenon has occurred in previous mode I fracture studies, but the reason is currently unknown. Weathering caused a slight, but significant decrease in G_{IC} and G_{IA} in poplar ($p=0.02$) and ($p=0.048$) respectively.

CHAPTER 4

SURFACE FREE ENERGY RELATIONS OF PMDI, SOUTHERN YELLOW PINE AND YELLOW-POPLAR----------

4.1 INTRODUCTION

Surface free energy analysis aids in our understanding of wood adhesion. Measuring the surface energies of the wood and the adhesive gives information about wetting, which is where adhesion begins. Over the past 40 years, several researchers have investigated the surface free energy of wood and wood adhesives with many methods (48). These methods are founded from the earlier work of surface scientists such as Young, Dupre, Zisman, Fowkes and others as we shall discuss.

In 1805 Thomas Young described how the contact angle of a liquid on a solid surface relates to the solid and liquid surface energies (4-1).

$$\gamma_{SV} = \gamma_{SL} + \gamma_{LV} \cos\theta \qquad 4\text{-}1$$

γ is the surface free energy and subscripts SV, SL and LV denote the solid-vapor, solid-liquid, and liquid-vapor interfaces respectively. Figure 4.1 illustrates the contact angle of a liquid on a solid as described by the Young equation.

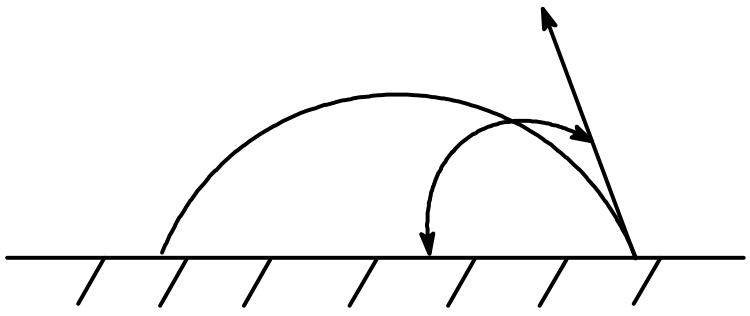

Figure 4.1 – Contact Angle of a Liquid on a Solid Substrate

Sixty years later, Dupre developed the concepts of work of cohesion and adhesion (free energy of adhesion). When two dissimilar bodies are brought together (adhesion), Dupre stated that the free energy of adhesion (ΔG^A) was:

$$\Delta G_{ij}{}^{A} = \gamma_{ij} - \gamma_i - \gamma_j \qquad 4\text{-}2$$

The free energy of adhesion represents the free energy change/unit area as substance *i* comes into contact with substance *j*. $\Delta G_{ij}{}^{A}$ is equal to the negative work of adhesion. The Young and Dupre equations are combined to describe the interfacial free energy in terms of the contact angle as follows:

$$\Delta G_{SL}{}^{A} = -\gamma_{LV}(1+\cos\theta) \qquad 4\text{-}3$$

One hundred years later Fowkes showed that surface energy can be separated into polar (γ^p) and non-polar (γ^d) components (49). Combining this information with the Young equation gives the geometric mean equation for calculating polar and non-polar components of surface energy.

$$(1+\cos\theta)\gamma_L = 2(\gamma^d{}_S\gamma^d{}_L)^{1/2} - 2(\gamma^p{}_S\gamma^p{}_L)^{1/2} \qquad 4\text{-}4$$

The polar surface energy can be further separated into acidic (γ_s^+) and basic (γ_s^-) components for the solid (49).

$$\gamma^p = 2(\gamma_s{}^+\gamma_s{}^-)^{1/2} \qquad 4\text{-}5$$

This allows the solid surface free energy (and its components) to be determined by measuring contact angles from liquids with known surface energies. This is known as the Lifshitz-van der Waals acid/base approach, which is expressed in equation 4-6 (49). LW stands for the non-polar component. In other words, using well characterized probe liquids, one can measure the wood surface energy (and its component energies).

$$(1+\cos\theta)\gamma_l = 2\left[(\gamma_s^{LW}\gamma_l^{LW})^{1/2} + (\gamma_s^{+}\gamma_l^{-})^{1/2} + (\gamma_s^{-}\gamma_l^{+})^{1/2}\right] \quad 4\text{-}6$$

This approach will be demonstrated in the following pages. This work investigates the surface free energy of two woods, southern yellow pine and yellow-poplar; and their surface interactions with pMDI. A Gibbs free energy of adhesion analysis was calculated for further insight into the differences in pMDI/pine, pMDI/poplar adhesion. Lastly, surface energy was measured on failure surfaces of DCB fracture specimens in order to gain some insight on adhesive performance.

4.2 LITERATURE REVIEW

4.2.1 Surface Energy of Wood

Gray was first to analyze the surface free energy of wood; he used the sessile drop contact angle (48). In his work, the critical surface tension (γ_c) was calculated from the Zisman method. It was found that critical surface tensions were in the range of 34.5 to 81.0 mJ/m^2, using the advancing angle; that is when the drop is actually spreading on the substance. One of the important findings was that freshly sanded surfaces were

approximately 20 mJ/m^2 higher in surface energy when compared to non-sanded, aged surfaces.

Consistent with Gray's findings, Nguyen and Johns also found that the surface free energy of wood decreased with aging time. Furthermore, Nguyen and Johns were the first to calculate the polar and non-polar components of wood surface energy utilizing the geometric mean and harmonic mean methods (51). Among their significant findings was the effect of extractives in Douglas fir and redwood. For example, they found that the total surface free energy of Douglas fir was 48.0 mJ/m^2 and extracted Douglas fir was 58.9 mJ/m^2. For redwood they found 54.2 mJ/m^2 for the total surface energy and 56.2 mJ/m^2 for extracted redwood. These results emphasize the role of extractives, and surface history (or aging) on wood surface energy.

Gardner compared the geometric mean and harmonic mean methods to the Lifshitz-van der Waals method for calculating surface energies (52). He also included the Zisman method in this comparison. Using polar and non-polar liquids it was shown that acid and base components of surface energy could be calculated for different wood species. Gardner concluded that the Lifshitz-van der Waals/acid-base approach more accurately determined the surface energy of wood. He determined this approach to be more reliable and robust compared to earlier methods described (49, 51). With the Lifshitz-van der Waals method, southern hardwoods used in his experiment had a total surface free energy between 40 and 54.3 mJ/m^2. Whereas the results with the geometric mean method were high, between 48 and 79 mJ/m^2. Harmonic mean results were between 46.3 and 63.4 mJ/m^2 and Zisman plot results were between 10.8 and 48.1 mJ/m^2.

Zisman results generally correlated well to the Lifshitz method, however some serious discrepancies were also noted.

Shen et al. investigated the surface energy of pine (Pinus silvestris L.) utilizing the Lifshitz-van der Waals/acid-base approach with dynamic and sessile drop methods (53). They found that component surface energies are dependent on the method used and also the grain orientation.

Among several, three methods are commonly employed to accurately measure wood surface energy. These include the sessile drop contact angle (48), dynamic contact angle (Wilhemy plate) (52,53) and inverse gas chromatography (IGC) (60). A fourth method used mainly by Gardner is the capillary wicking method. Both IGC and wicking methods rely on wood powder, which will give different results than measurements on solid wood.

Gardner characterized surface energies of wood particles with dynamic contact angle, capillary wicking and IGC. It was found that the IGC dispersive surface energy was higher than dynamic contact angle results. Capillary wicking results show that it is an effective method for measuring the dispersive surface energy. Acidic/basic surface energy measurements using IGC were complicated by negative enthalpy of special adsorption with certain probes (60).

Sessile drop contact angle analysis was used to determine surface free energy for all parts of this study. In part one, the surface free energy components (Lifshitz-van der Waals, acid and base) of pine and poplar tangential surfaces were examined. This was done to study the correlation between surface energy and adhesion. Secondly, the free energy of adhesion (ΔG^A) was calculated for both the poplar/pMDI and pine/pMDI

systems. Lastly, the surface free energy of failure surfaces from fracture test specimens was measured, mostly for curiosity, but in an attempt to gain some insight on pMDI/wood bonding.

4.3 SAMPLE PREPARTATION

Specimens for surface analysis were taken from wood laminae cut and conditioned for mode I fracture testing. Details of mode I fracture cleavage sample preparation were mentioned in Section 3.3. The average distance between growth rings for pine was 4.3mm (2-7mm range) and was 12mm (8-17mm range) for poplar. Latewood width in pine averaged 2mm (1-5mm range) and in poplar it was less than 0.5mm (up to 0.5mm). Contact angle measurements were taken within one hour of planning with the camera perpendicular to the longitudinal wood axis. Samples were stored in a zip lock bag until used. Approximately half the measurements performed on earlywood and half on latewood and the results were averaged. Measurements taken on the fracture surface of failed DCB specimens were taken between crack extensions of 50 and 150mm. Contact angles were measured within thirty minutes after fracture testing. The fractured bondline was kept intact until just prior to testing.

Five probe liquids were used to investigate wood surface energies of both poplar and pine. The surface free energy components of the liquids are given in Table 4.1 (49).

Table 4.1 – Surface tension components of probe liquids at 20°C (mJ/m^2).

Liquids	γL	γ^{LW}	γ^+	γ^-
α-bromonapthelene	44.4	44.4	0	0
Ethylene Glycol	48	29	1.92	47
Formamide	58	39	2.28	39.6
Glycerol	64	34	3.92	57.4
Water	72.8	21.8	25.5	25.5

4.4 TEST PROCEDURE

Measurements were made on tangential wood surfaces. A 10 μL drop was applied to the wood surface with a volumetric pipette. The sessile drop contact angle was recorded with a digital video image analysis system. The sample image was recorded 0.5 seconds after liquid contact. The image analysis software captures the digital image and allows contact angle measurement with tools available in the software package. Six panels of each species were used for measurements; five contact angles with each liquid were measured on each. Additionally, seven contact angle measurements with pMDI were performed on each species. Three DCB fracture specimens of each species were tested. Each fractured surface (six surfaces for each species) was measured with one drop of each liquid.

4.5 RESULTS AND DISCUSSION

4.5.1 Surface Energy of Pine and Poplar

The surface free energy was measured on six panels for each species. The average contact angle for each panel is given in Table 4.2. Close investigation reveals differences within and between species.

Table 4.2 – Average contact angle for pine and poplar panels

Sample	α-bromonapthalene	Water	Glycerol	Ethylene Glycol	Formamide
Pine 1	18 (3)*+	28 (6)	69 (6)	28 (2)	22 (3)
Pine 2	22 (6)	31 (4)	77 (3)	31 (5)	19 (3)
Pine 3	25 (2)	32 (6)	76 (9)	31 (3)	21 (4)
Pine 4	19 (4)	34 (2)	72 (6)	29 (4)	18 (3)
Pine 5	18 (3)	33 (2)	73 (9)	28 (2)	18 (2)
Pine 6	17 (3)	40 (5)	73 (5)	28 (2)	21 (3)
Poplar 1	9 (1)	52 (6)	58 (2)	22 (6)	12 (4)
Poplar 2	13 (2)	47 (5)	58 (4)	17 (8)	14 (3)
Poplar 3	11 (2)	42 (3)	54 (2)	21 (3)	12 (2)
Poplar 4	11 (2)	41 (5)	55 (5)	19 (1)	13 (4)
Poplar 5	10 (2)	47 (3)	63 (2)	19 (3)	15 (2)
Poplar 6	10 (2)	48 (4)	62 (4)	20 (4)	16 (3)

*Standard deviation appears in parenthesis +n=5 for each mean

It is interesting to consider the surface energies of the probe liquids (Table 4.1) and the resulting contact angles (Table 4.2). The contact angle of water was significantly lower than glycerol with both species, even though the surface tension of water is higher. Gardner's work had similar results (52). This demonstrates that the wood wetting behavior of water and glycerol is not completely explained by γ^L. If it were, the glycerol would wet better. Instead, these results suggest that wetting is affected by specific interactions. In other words, the surface energy components (γ^{LW}, γ^+, γ^-) appear to have a significant affect.

Surface free energies for wood and wood fracture cleavage surfaces were calculated according to the Lifshitz-van der Waals acid/base approach (52). This allows calculation of the total solid surface energy, along with the non-polar, acid (γ_s^+) and basic (γ_s^-) components. This approach uses 1 non-polar and 4 polar liquids for measuring the contact angles. Each liquid's energy components are known and the contact angle of each liquid/sample combination is measured. Consequently, using equation 4-7 a set of 5

simultaneous equations are used to calculate the sample surface free energy and its components (52). Each panel's results were averaged and the total surface energy was calculated with equation 4-8. Results are given in Table 4.3

$$(1+\cos\theta)\gamma_l = 2\left[(\gamma_s^{LW}\gamma_l^{LW})^{1/2} + (\gamma_s^{+}\gamma_l^{-})^{1/2} + (\gamma_s^{-}\gamma_l^{+})^{1/2}\right] \quad 4\text{-}7$$

$$\gamma^T = \gamma_s^{LW} + (2(\gamma_s^{+}\gamma_s^{-})^{1/2}) \quad 4\text{-}8$$

Table 4.3 – Overall surface energy results of pine and poplar.

Species	Non-polar	Acidic	Basic	Total Surface Energy
Yellow Poplar	44.0 (0)	0.80 (0.10)	30.9 (4.9)	53.7 (0.5)
Southern Yellow Pine	41.8 (0.80)	1.4 (0.3)	59.3 (6.1)	60.0 (1.2)

The results show that pine had a significantly higher total surface free energy. The higher total surface free energy was due to significantly higher acid and base surface energy components. Average and standard deviation was calculated from the surface energy of each wood panel given in Table 4.2. Yellow-poplar had a significantly higher non-polar surface energy component. These results indicate that pine has a higher surface free energy than poplar, suggesting that pMDI may wet better on pine than on poplar. However, this was not the case. Table 4.4 shows that the wetting of pMDI was no different on pine or poplar. However, notice that the component surface energies are different for the woods (Table 4.2). Recall how liquid component surface energies affected the wetting of wood. Is it possible that the component surface energies of wood are affecting adhesion in complex ways? One way to investigate this theoretically is a Gibbs free energy of adhesion analysis.

Table 4.4 – Contact angle of pMDI on each species.

Species	Contact angle[+]
Yellow-poplar	32.2
Southern yellow pine	32.5

+ n=7

4.5.2 Free Energy of Adhesion

The free energy of adhesion (ΔG^A) is defined as the free energy change per unit area when two substances are brought into contact (54). Many researchers have correlated the free energy of adhesion with mechanical properties of bonded assemblies (55).

Eley derived an equation to evaluate the energy change needed to separate two solids *i* and *j* in a liquid medium (54).

$$\Delta G_{ijL} = -(\gamma_{iL} + \gamma_{jL} - \gamma_{ij}) \qquad 4\text{-}8$$

For adhesion in an air medium (wood bonding), the adhesive acts as the liquid medium. This is illustrated in Figure 4.2.

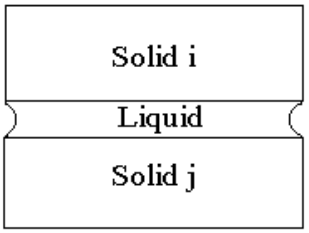

Figure 4.2 – Interaction of two solids i and j separated by a liquid medium (L).

In this relation the free energy of adhesion is ΔG_{ijL}, γ_{iL} is the surface energy of the solid *i*/liquid interface, γ_{jL} is the surface energy of the solid *j*/liquid interface and γ_{ij} is the theoretical surface energy of the solid/solid interface, which consists of the Lifshitz-van der Waals component (γ_{ij}^{LW}) and acid/base component (γ_{ij}^{AB}).

$$\gamma_{ij} = \gamma_{ij}^{LW} + \gamma_{ij}^{AB} \qquad 4\text{-}9$$

$$\gamma_{ij}^{LW} = \gamma_i^{LW} + \gamma_j^{LW} - 2(\gamma_i^{LW}\gamma_j^{LW})^{1/2} \qquad 4\text{-}10$$

$$\gamma_{ij}^{AB} = 2[(\gamma_i^{+})^{1/2} - (\gamma_j^{+})^{1/2}][(\gamma_i^{-})^{1/2} - (\gamma_j^{-})^{1/2}] \qquad 4\text{-}11$$

Expanding the components of γ_{ij} we get the following expression:

$$\gamma_{ij} = \gamma_i^{LW} + \gamma_j^{LW} - 2(\gamma_i^{LW}\gamma_j^{LW}) + 2[(\gamma_i^{+})^{1/2} - (\gamma_j^{+})^{1/2}][(\gamma_i^{-})^{1/2} - (\gamma_j)^{1/2}] \qquad 4\text{-}12$$

The interfacial solid/liquid surface free energies, γ_{iL} and γ_{jL} are derived from Young's equation:

$$\cos\theta = (\gamma_{SV} - \gamma_{SL}) / \gamma_{LV} \qquad 4\text{-}13$$

γ_{SV} is the surface energy of the solid/vapor interface, γ_{SL} is the surface energy of the solid/liquid interface and γ_{LV} is the surface energy of the liquid/vapor interface.

Therefore: γ_{iL} *(or* γ_{jL}*)* $= \gamma_{iV} - \gamma_{LV}\cos\theta$ 4-14

Since $\gamma_{iV} = \gamma_i^{LW} + 2(\gamma_i^{+}\gamma_i^{-})^{1/2}$, the relation by Eley (5-1) can be rewritten:

$$\Delta G_{ijL} = \gamma L(\cos\theta_{iL} + \cos\theta_{jL}) - 2[\gamma_j^{LW}\gamma_i^{LW})^{1/2} + (\gamma_i^{+}\gamma_j^{-})^{1/2} + (\gamma_i^{-}\gamma_j^{+})^{1/2}] \qquad 4\text{-}15$$

A free energy of adhesion analysis was performed for the pine/pMDI and for the poplar/pMDI systems (Equation 4-15). Liquid pMDI surface energy at 25°C was unknown, therefore the value was extrapolated from known values at higher temperatures using an industrial resin from Dow. The extrapolation is shown in Figure 4.3 (27).

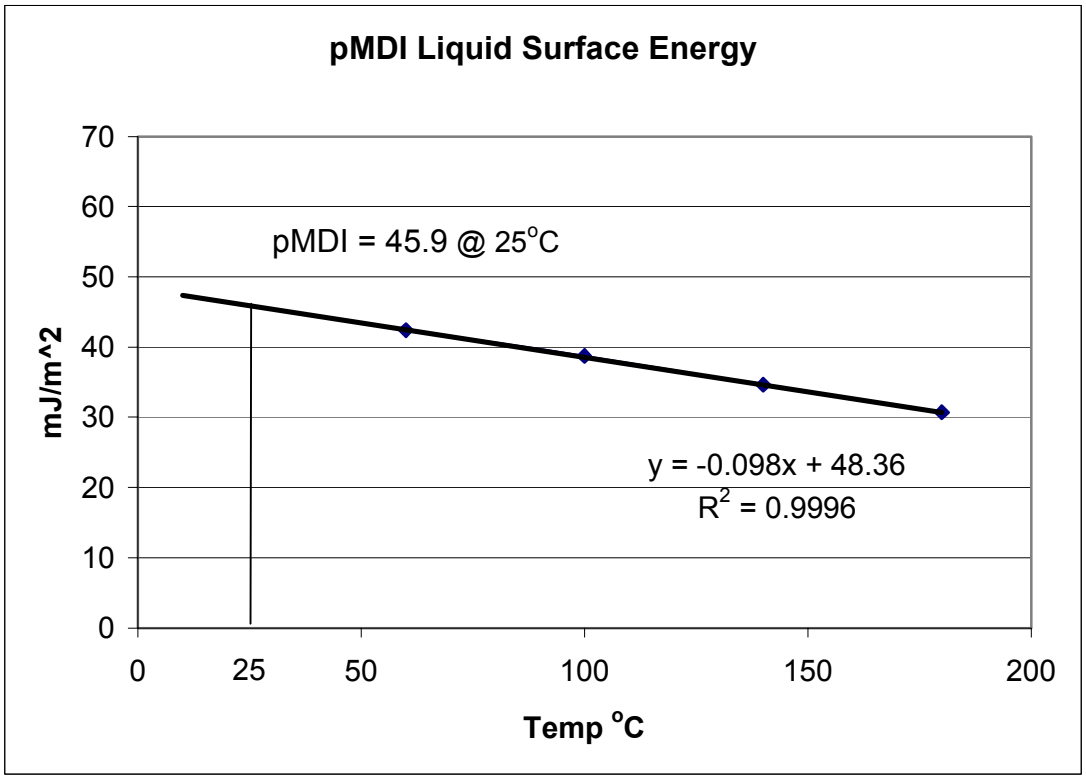

Figure 4.3 – Extrapolated surface free energy of pMDI (27)

The pMDI surface energy was determined to be 45.9 J/m^2 from this extrapolation. The contact angle of pMDI was measured on pine and poplar surfaces. Table 4.5 presents the contact angle and the free energy of adhesion results. Table 4.5 shows a lower ΔG^A for pine, meaning that the adhesive force is greater. The reader should note that this calculation only gives us information about the system before cure. After cure each system will change dramatically because of the transformation of the

pMDI adhesive from low molecular weight liquid to a high molecular weight extensively cross-linked solid.

Table 4.5 – Contact angles of pMDI and free energy of adhesion on each species

Species	Contact Angle	ΔG (mJ/m^2)
Yellow-poplar	32.2	-27.0
Southern Yellow Pine	32.5	-38.2

Recall from section 4.5.1 when we discussed the effect of surface energy components. Water wet better than glycerol, even though it had a higher total surface energy. This indicated that the wetting effect was dependent on the total surface energy as well as the components. The pMDI contact angle on both woods was equivalent. This is counterintuitive because pine had a significantly higher surface energy and therefore pMDI should wet better. Is it possible that the components of surface energy are playing a significant role, but that we cannot visually observe the effect in the contact angle?

The strength of the Gibbs free energy analysis is that we can look at the effect of the surface energy components compared to the liquid surface tension and contact angle. We know from the ΔG analysis that there is more energy available for adhesion with the pine/pMDI system. This is consistent with the fracture test findings presented earlier – pMDI adhesion to pine was better than to poplar. While this is simply conjecture, it may be that the superior adhesion to pine is the result of specific interactions that are evident from the adhesion free energy analysis. But again, any evidence of specific interactions in the pine/pMDI system, which are absent in the poplar system, are not evident from the observed wetting of pMDI on pine and poplar; the contact angles are the same.

4.5.3 Surface Free Energy of Pine and Poplar Fracture Surfaces

In order to learn about the failure surfaces, additional pine and poplar DCB's were prepared and tested. DCB samples were prepared and tested for the sole purpose of measuring the surface energy of the fracture surfaces. Fracture cleavage testing was performed on one lamina each of poplar and pine. The southern pine had significantly higher G_{IC} and G_{IA} energies than yellow-poplar (Table 4.6). This is consistent with results presented earlier.

Table 4.6 - Fracture Energies of Samples used in Surface Measurements

Species	**G_{IC}**	**G_{IA}**	**Specimens**	**Cycles**	**Adhesive coverage (g/m^2)**
Yellow-poplar	170.8	146.8	3	31	172
Southern Yellow Pine	262.2	234.5	3	41	102

Immediately after fracture testing, contact angles of the five liquids were performed on each of the fracture surfaces. The contact angle results are given in Table 4.6. The resulting calculated surface free energy component results are given in Table 4.7.

Table 4.6 – Contact angle results for pine and poplar fracture surfaces (n=6)

Species	Glycerol	Formamide	Water	Ethylene Glycol	α-bromonapthelene
Yellow-Poplar	43.6 (3.0)*	28.2 (6.4)	42.1 (3.2)	26.2 (3.6)	1.9 (1.6)
Southern Yellow Pine	40.6 (5.7)	19.1 (6.9)	32.0 (5.1)	22.1 (5.1)	4.3 (2.6)

* Standard deviation is located in the parenthesis

Table 4.7 - Surface energy parameters of pine and poplar fracture surfaces

Species	γ_s^{LW}	γ_s^{+}	γ_s^{-}	γ_s^{Total}
Yellow-Poplar	44.4	0.3	35.0	50.8
Southern Yellow Pine	44.4	0.4	51.9	52.9

Note that the pine and poplar failure surface energies are very similar, with the exception of the basic components. The basic component was significantly higher on the pine surface. Finally, it is interesting to compare the surface energies of the failure surfaces to the corresponding freshly machined surfaces (Table 4.3). The reader is left to consider the implications.

4.6 CONCLUSION

Contact angles were measured on the tangential surfaces of freshly machined southern yellow pine and yellow-poplar. The Lifshitz-van der Waals approach was used to calculate surface energy from these contact angles for both species. Pine had a significantly higher total surface free energy than yellow-poplar. Higher acid and base components of surface energy were also observed in pine. This indicates pMDI should wet pine surfaces better than poplar; but this was not the case. This may also suggest that pMDI adhesion should be better with pine as opposed to poplar. In fact, fracture testing supports this conclusion. Fracture results with pMDI bonded laminates showed a significantly higher fracture energy with pine over yellow-poplar.

The free energy of adhesion (ΔG) was analyzed in the pine/pMDI and poplar/pMDI systems. The system measured was from data obtained in the uncured state, which may not accurately represent the cured pMDI/wood system. ΔG was calculated from the surface energy components of each species, the surface free energy of the adhesive and the contact angle of pMDI on each substrate. It was shown that the pine/pMDI system would require more energy for separation. Fracture cleavage results reflect this correlation. This study indicates that pMDI/wood species adhesion could be dependent on surface component interactions.

The surface free energy of fresh fracture cleavage surfaces was measured. It was shown that the pine/pMDI surface had a slightly higher total surface energy than the poplar/pMDI surface. Fracture surfaces on pine and poplar had equal non-polar and acidic components of surface energy. The fractured pine surface had a significantly higher basic component of surface energy. The surface free energy of the poplar and pine fracture surfaces were lower, but similar to the surface free energy of the individual wood species. It could be theorized that the fracture surface energy is dictated by the surface energy of the substrate.

CHAPTER 5

SYNTHESIS OF DOUBLY LABELED POLYMERIC MDI for SOLID-STATE NMR STUDIES----------

5.1 INTRODUCTION

The efficiency of pMDI as a wood binder has lead to a plethora of fundamental research into isocyanate/wood cure chemistry. The reactive nature of the isocyanate functional group enables it to bond to wood nucleophiles by addition reactions. Prior research to investigate the cure chemistry of pMDI adhesives with wood has used FTIR and ^{15}N CP/MAS NMR (8-14, 20, 22-26). These studies have shown the formation of urea, biuret and possible urethane linkages in the wood/isocyanate bondline. These methods have struggled to clearly identify and quantify the amount of covalently bonded material present (urethane). Urethane formation is important, because adhesive bonds with urethanes should have better durability than bonds without. FTIR has been limited by the effect of wood on the signal in the carbonyl region. In nitrogen-15 solid-state NMR studies, signal overlap between the urea and urethane linkages has limited its effectiveness. This is illustrated in Figure 1.1. The urethane (bottom) signal at 101ppm is overlapped by the urea and signal (top) in the wood composite at 7% MC.

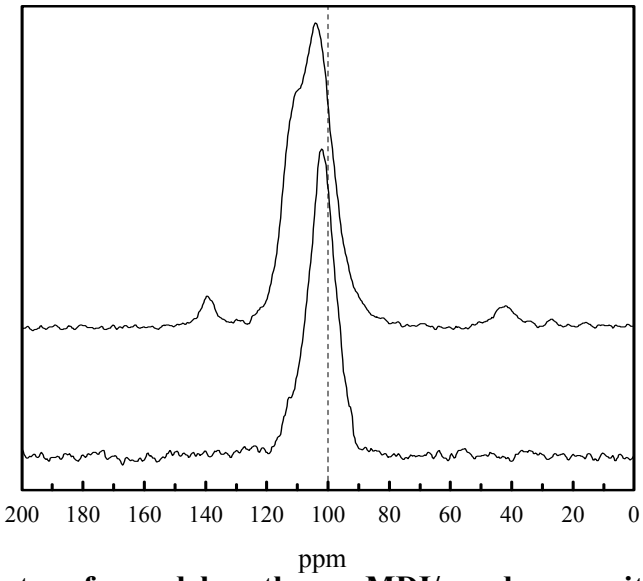

Figure 5.1 – ^{15}N spectra of a model urethane pMDI/wood composite (bottom) and typical pMDI/wood composite at 7% MC showing the effect of signal overlap (Taken from Zhou and Frazier, 2001).

Clearly identifying urethane linkages would aid researchers to gain a fuller understanding of pMDI bonding efficiency. Recently a procedure for using a pMDI-^{13}C, ^{15}N adhesive was developed by Zhou and Frazier (56). Both labeled isotopes were synthetically inserted into the isocyanate group. Their research with yellow-poplar provided strong evidence for the existence of urethane linkages in lab scale composites.

This research was primarily directed towards the optimization of the synthesis of pMDI-^{13}C, ^{15}N adhesive. Secondly, labeled adhesive was used in manufacture of 2-ply composites to elucidate cure chemistry between pine/pMDI and poplar/pMDI.

5.2 LITERATURE REVIEW

5.2.1 Polyamine Synthesis

pMDI synthesis requires two steps: 1) The HCl catalyzed condensation of aniline and formaldehyde to form methylene dianilines and higher polyarylamines, and 2) the phosgenation of these amines to form the corresponding isocyanates. The synthesis of the polyamine is thoroughly reviewed by both Twitchett (47) and Ulrich (48). Figure 5.2 gives the overall reaction scheme.

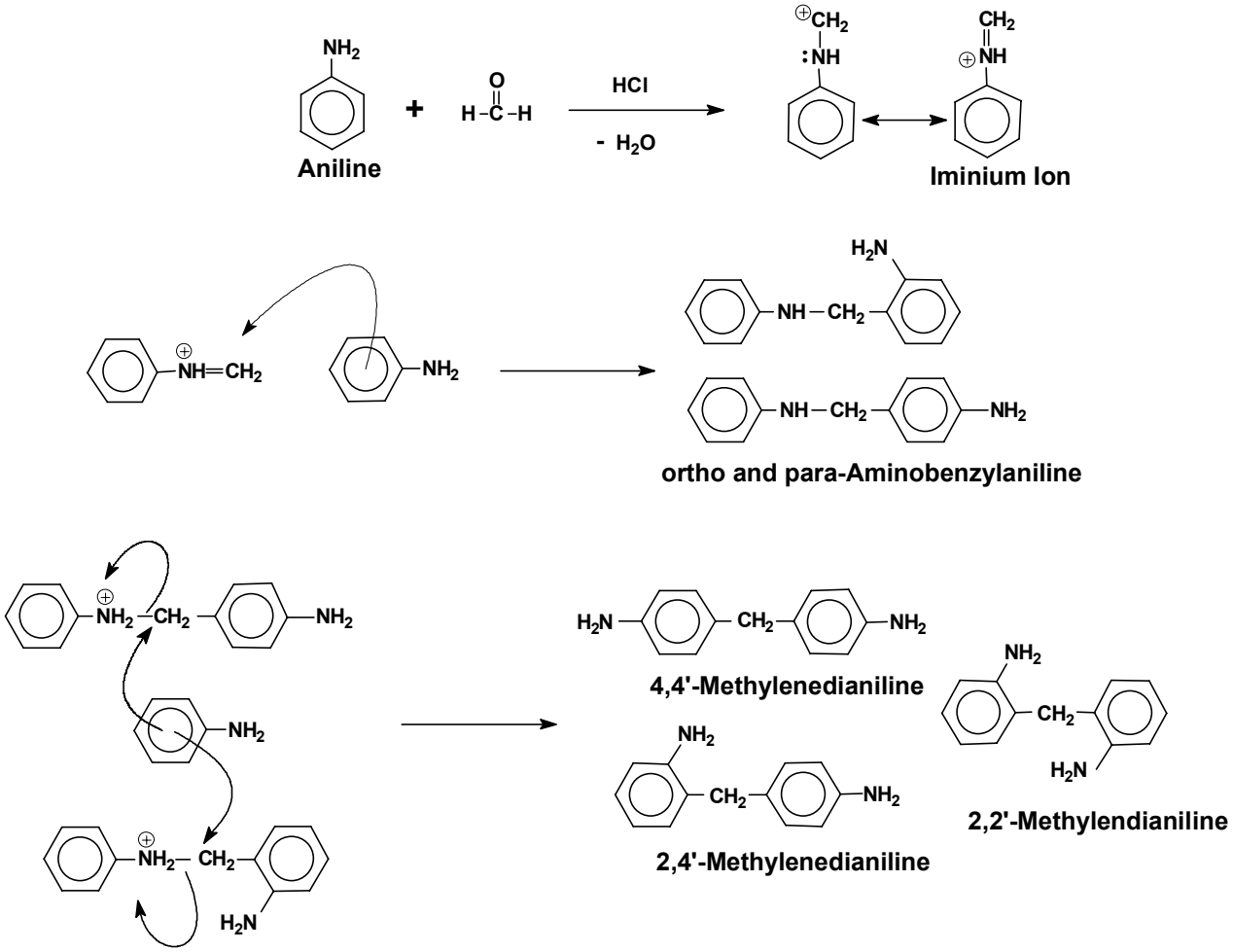

Figure 5.2 – Reaction scheme of the HCl catalyzed aniline : formaldehyde condensation.

The first stage of the polyamine reaction occurs with the addition of formaldehyde to aniline under acid conditions. Iminium ions (electrophile) form with the elimination of water. This electrophile substitutes into the aromatic ring of aniline to form ortho- and para-aminobenzylaniline. Iminium ions can also react with higher polyamines, to form the corresponding aminobenzylanilines. In the second step, called the "isomerization stage", aminobenzylaniline reacts with aniline in another electrophilic aromatic substitution. This reaction forms 4,4'-methylenedianiline and a lesser amount of 2,2' and 2,4' methylene dianiline. Side reactions can form up to seven kinds of isomeric triamines and fifteen types of tetraamines. If the reaction occurs with a molar excess of acid to aniline, the side reactions can be retarded. Approximately half of the aniline used in the reaction is consumed. This holds true with high or low aniline:acid mole ratios, because the formaldehyde reacts swiftly to convert diamines into triamines. Six principal factors affect polyamine composition (7):

1) Aniline:Formaldehyde ratio
2) Aniline:HCl ratio
3) Reactant Concentration
4) Temperature
5) Rate of addition of Formaldehyde
6) Pressure

5.2.2 Phosgenation of Polyamines

Hentschel first phosgenated arylamines to synthesize isocyanates in 1884 (48). Industrially, aromatic isocyanates are formed from the continuous reaction of aromatic amines with an excess of phosgene in chlorobenzene (19). In laboratory use, aromatic amines are added to an excess of phosgene in chlorobenzene or ODCB below 20°C. Carbamoyl chlorides and amine hydrochloride form instantly with vigorous agitation. At 70°C carbamoyl chlorides eliminate HCl to form isocyanates. Complete phosgenation of the amine hydrochloride occurs at the boiling point of the solvent used.

Polymeric methylenebis(phenylisocyanate) (pMDI) is produced as described above. On average each pMDI molecule contains 2.8 functional groups (NCO). The overall pMDI reaction is given in Figure 5.3.

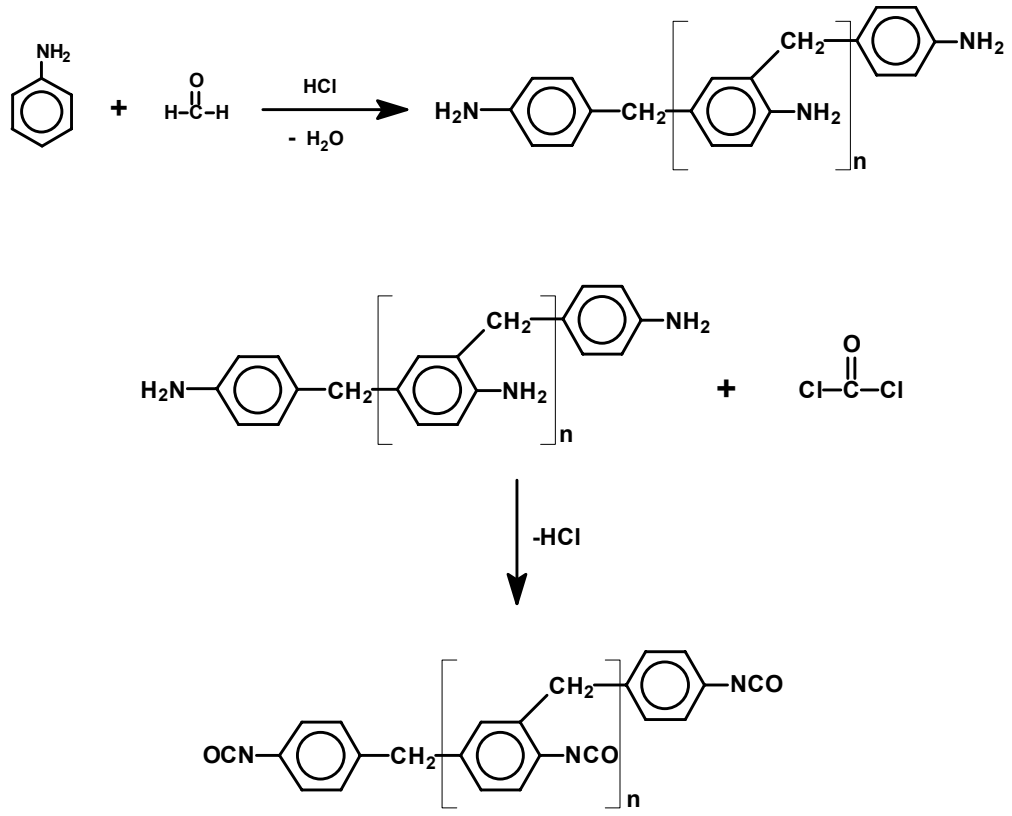

Figure 5.3 – Two-step synthesis of pMDI.

5.2.3 Phosgene Synthesis

Davy first prepared phosgene in 1812 from the photochemical reaction of carbon monoxide and chlorine gas (57). Phosgene was widely known for its use as a WWI warfare agent, but its principle uses today are in the formation of isocyanates, polycarbonates, chloroformates and carbonates.

Phosgene is a colorless gas with a boiling point of 7.48°C. Phosgene forms a white solid at temperatures below –127.84°C. It is soluble in aromatic and aliphatic hydrocarbons, chlorinated hydrocarbons, esters and organic acids. It has a high toxicity

(LSD=50ppm) and its olfactory detection occurs at levels as low as 0.5ppm (57). It reacts readily with many compounds including: water, alcohols, phenols and primary and secondary amines. Phosgene reactions with primary amines are important for isocyanate synthesis.

Phosgene is produced industrially by the reaction of chlorine with carbon monoxide in the presence of activated carbon catalyst. This is a gas phase reaction, but phosgene can also be synthesized in solution (19). Typical solvents used include: chlorobenzene, 1,2-dichlorobenzene (ODCB) and 1,2,4-trichlorobenzene. Chlorinated solvents are preferred to prevent chlorine from reacting with the solvent. Figure 5.2 shows the overall reaction.

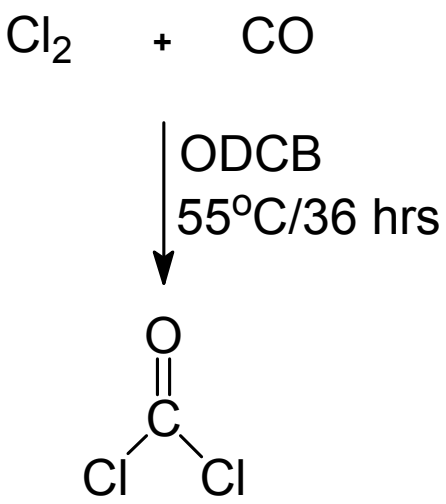

Figure 5.4 – Phosgene reaction from chlorine and carbon monoxide.

5.2.4 ^{13}C, ^{15}N PMDI

Zhou and Frazier were the first to synthesize a doubly labeled pMDI-^{13}C, ^{15}N resin, with both labels in the isocyanate functional group (56). Their resin had similar characteristics to industrial pMDI. This was done to elucidate the cure chemistry of

pMDI with wood. Figure 5.5 shows ^{15}N spectra of a model urethane pMDI/wood composite (bottom) and a typical pMDI/wood composite at 7% MC (top). The urethane signal appears at 101 ppm; prior research has shown that the urea resonates at 104ppm as demonstrated in the top spectrum of Figure 5.5.

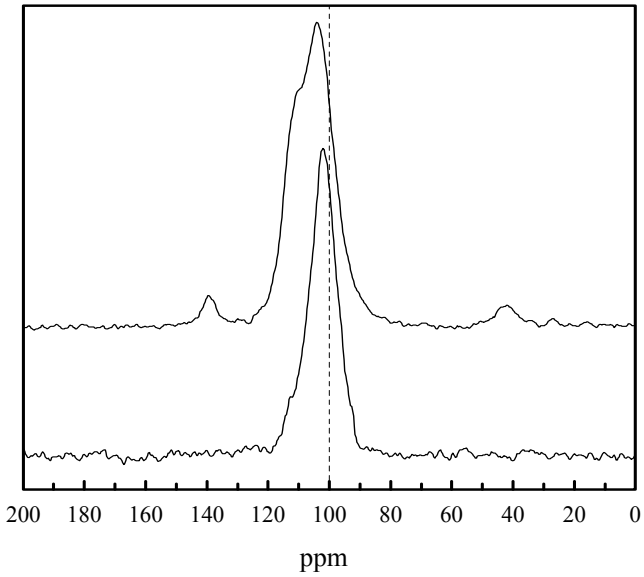

Figure 5.5 – ^{15}N Spectra of a model urethane pMDI/wood composite (bottom) and Typical pMDI/wood composite at 7% MC showing the effect of signal overlap (Taken from Zhou and Frazier, 2001).

It can be seen that signal overlap prevents the unambiguous detection of urethane. Zhou and Frazier have shown that this problem can be overcome through the use of doubly labeled resin, pMDI-^{13}C, ^{15}N. Figure 5.6 shows NMR spectra of wood composites with no resin (bottom), ^{13}C labeled pMDI/wood (top) and double-labeled pMDI/wood (middle). The important section of the spectra occurs in the carbonyl region (150ppm-156ppm), where urethanes, ureas, and biuret carbonyls resonate. The top spectrum shows that the signal broadening with only a ^{13}C label gives no information on

cure chemistry. The middle spectrum of the double-labeled composite provides information that is not seen with only C13 labeling. Apparently, the N15 nucleus eliminates N14 quadrupolar broadening of the carbon signal. The result is structural detail in the form of a sharp maximum at 156 ppm, and a broad shoulder at 154 ppm. Zhou and Frazier identified the maximum at 156 as the urethane. While the double label still does not provide clear resolution of urea and urethane, the combination of the information from the N15 and C13 spectra now provides the clearest evidence for urethane formation in the wood/pMDI bondline (56). Biurets and ureas were identified as the shoulder appearing at 151-154 ppm.

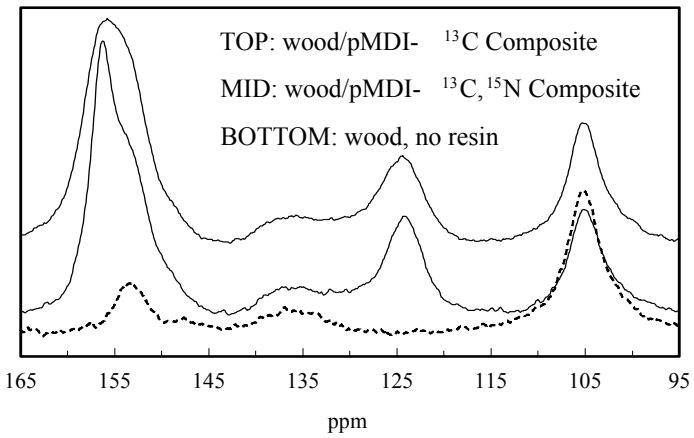

Figure 5.6 – Solid-state NMR spectra for wood, ^{13}C pMDI/wood composites and ^{13}C, ^{15}N pMDI/wood composites showing the clear determination of urethane at 155ppm in the middle spectrum (Taken from Zhou and Frazier, 2001).

The purpose of the following research was to optimize the synthesis of pMDI ^{13}C, ^{15}N adhesive. Secondly, 2-ply composites were manufactured use for solid-state NMR studies that are not described here.

5.3 REAGENTS

Nitrogen

Ultra pure nitrogen was regulated through a gas purifier filled with anhydrous calcium sulfate. A regulator at the tank head controlled the dried nitrogen flow rate. Dried nitrogen ran through a nitrogen/vacuum manifold fitted with glass stopcocks. The vacuum portion of the manifold was connected to a Fisher Maxima C Plus Model M2C mechanical vacuum pump with an in-line cold trap and monometer.

5.3.1 Polyamine Synthesis

Aniline. Aniline (Aldrich Chemical) was used as received.

99% ^{15}N-enriched Aniline. 99% ^{15}N-enriched aniline (Cambridge Isotope Laboratories, Lot PR-10950) was used as received. The labeled material was a dark brown color indicating the presence of impurities.

The following items were used as received:

Paraformaldehyde. (Fisher Chemical)

37% Aqueous hydrochloric acid. (Fisher Chemical).

Chloroform. (EM Science Certified A.C.S., HPLC grade)

Distilled Water.

10N Sodium hydroxide. (NaOH) (Fisher, Certified)

5.3.2 Phosgene Titration

Acetone. Acetone (Aldrich Chemical, Reagent Grade 99.7%) was dried for 24 hours with molecular sieves before use.

Sodium Iodide. NaI (Aldrich Chemical) was stored under nitrogen gas and used dry.

Sodium Thio Sulfate Pentahydrate. $Na_2S_2O_3 \cdot 5H_2O$ was used as received.

5.3.3 Polyamine Phosgenation

1,2-Dichlorobenze. Anhydrous 1,2-dichlorobenzene (ODCB) (Aldrich Chemical) was used as received.

Chlorine. Chlorine gas (Cl_2) 99.5% pure (Aldrich Chemical) was used as received and controlled with a regulator at the tank head.

Carbon Monoxide. Carbon Monoxide gas (CO) 98% pure (Aldrich Chemical) was used as received and controlled with a regulator at the tank head.

99% ^{13}C-labeled Carbon Monoxide. 99% 13C-labeled Carbon Monoxide gas 98% pure (Cambridge Isotope Laboratories, Lot 7675 102B) was used as received and controlled with a regulator at the tank head.

5.3.4 Isocyanate Titration

Dibutylamine. Dibutylamine (Aldrich Chemical) was used as received.

Toluene. Toluene (Aldrich Chemical) was used as received.

Methanol. Methanol (Allied Signal) 99.9+% pure was used as received.

1,2,4-Trichlorobenzene. Anhydrous 1,2,4-Trichlorobenzene (Aldrich Chemical) was used as received.

0.04 wt. % Bromophenol Blue. 0.04 wt. Percent in water Bromophenol Blue

5.4 SYNTHESIS OF POLYMERIC MDI

5.4.1 Polyamine Synthesis

Aniline-^{15}N (10g, 0.108mol) was added dropwise to 6N HCl (26.5ml, 0.172mol) in a 100ml triple neck round bottom flask containing a magnetic stir bar. The flask was immersed in an ice bath to quench the exotherm. Paraformaldehyde (0.81g, 0.027mol) was slowly stirred into the acid/aniline mixture while maintaining the ice bath. A condenser was attached to the triple neck flask and the flask was lowered into a silicon oil bath, which was heated to 120°C. The ingredients were refluxed for eight hours with moderate stirring. Once cooled, the aqueous solution was poured into a 250ml separation funnel containing 25ml of HPLC grade chloroform. 10N NaOH was added until the aqueous phase became basic. The organic phase was isolated and the remaining aqueous phase was extracted twice with chloroform (2x25ml). The organic phases were combined and washed twice with distilled water. Chloroform was evaporated from the product. Water and residual aniline were removed by vacuum distillation at 0.1mmHg at 60°C; the temperature was increased by increments of 10°C until all signs of aniline condensation disappeared.

5.4.2 Phosgene Synthesis

Chlorine gas (8.52g, 0.12mol) from a 50L lecture bottle was dissolved into 150ml of anhydrous 1,2 dichlorobenzene (ODCB) at atmospheric conditions under a nitrogen blanket. The chlorine gas was controlled with a Monel (chemical resistant alloy) lecture-bottle control valve and passed through chemically resistant Tygon R-3400. The tubing

was connected to a specially made glass adaptor fitted into a 250ml-graduated cylinder with a 24/40 neck (Figure 5.7). Chlorine addition was

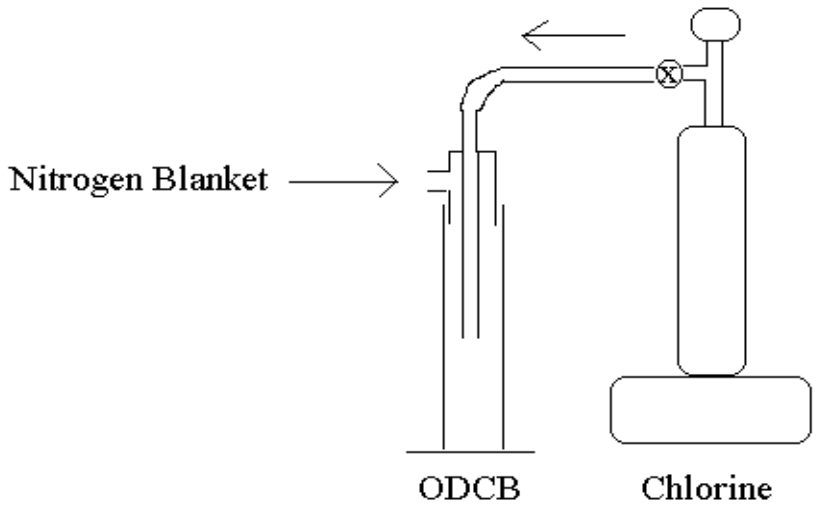

Figure 5.7 – Chlorine addition into ODCB under dry conditions

monitored gravimetrically. Once the correct amount of chlorine was in solution, a septum was applied to the graduated cylinder under a nitrogen blanket. The volume increase with 8.52g of chlorine was approximately 3 to 4 milliliters.

A five-necked 3L reaction kettle (Ace glass, medium pressure glass reactor) was flame dried under nitrogen and purged with vacuum and nitrogen three times. The purged kettle was filled with ^{13}CO (2.9L, 0.12mol)

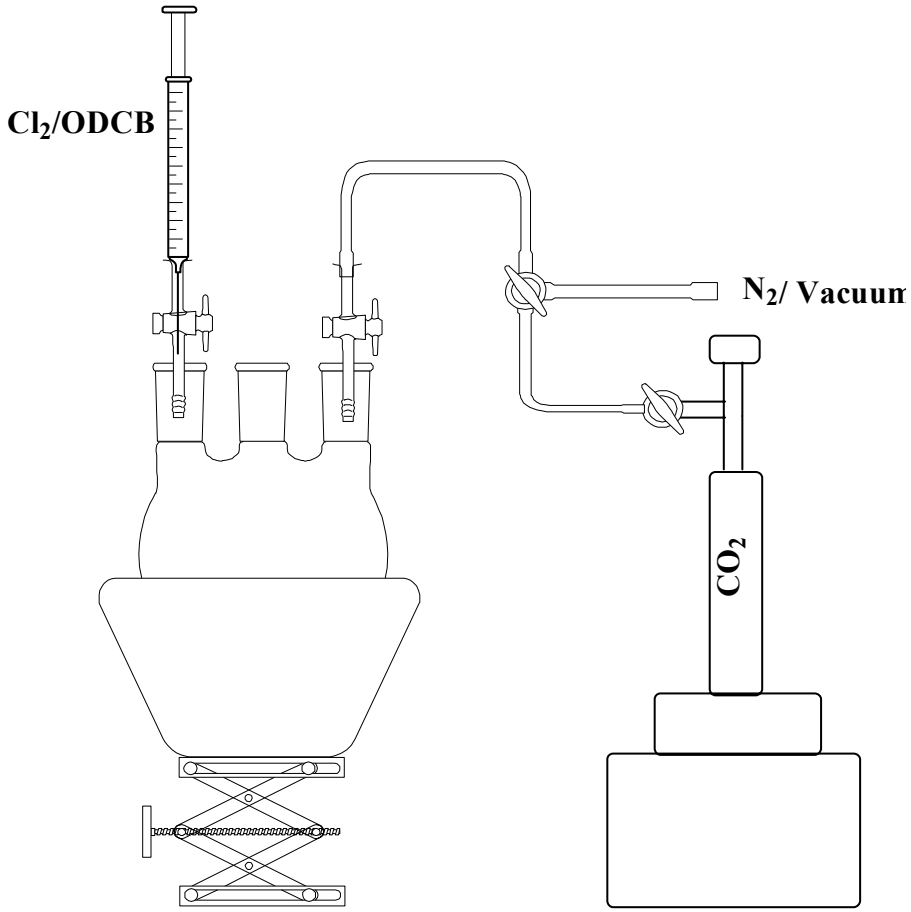

Figure 5.8 – Glass apparatus used for phosgene synthesis

Carbon monoxide addition was monitored with a bubbler. The chlorine/ODCB solution was injected into the kettle containing the carbon monoxide with a 60ml disposable syringe. Nitrogen gas pressure was used to transfer the chlorine/ODCB solution from the graduated cylinder into the syringe. It took three injections to transfer all of the solution.

The mixture was vigorously stirred for forty-eight hours on a stirring hot plate in a silicone oil bath at 60°C. The oil bath was preheated to approximately 35°C to 40°C before the injection. When the reaction was finished, the kettle was cooled to room

temperature. The final product was a translucent yellow. Cyclohexene (10ml) was injected into the flask to react with residual chlorine, for one hour with vigorous stirring. The phosgene solution sometimes turned into a translucent gold and other times pink after the reaction was finished. No correlation was made between this color and the final yield.

- **Phosgene Purification**

The contents of the reaction kettle were placed under a nitrogen blanket, and the kettle was immersed in an ice bath. A trap was flamed under nitrogen and connected to the reaction kettle with R-3603 Tygon tubing; the nitrogen blanket was closed to the reaction kettle, simultaneously. The trap was immersed into liquid nitrogen and a vacuum (~1mmHg) was pulled through the trap onto the moderately stirred phosgene solution. Phosgene transfer was observed and controlled by monitoring the bubble formation in the 3L reaction kettle. Bubbling was very mild to prevent phosgene from escaping into the manifold. The purification took approximately ten minutes until bubble formation stopped. The vacuum was pulled on the solution for an additional five minutes and then the transfer was complete. Phosgene was observed as a pure white solid. One hundred milliliters of anhydrous ODCB was carefully syringed into the trap while still immersed in liquid nitrogen. During this addition, nitrogen was intermittently added into the trap through the reaction kettle to alleviate pressure. Once all of the ODCB was added to the phosgene, the trap was taken out of the liquid nitrogen and allowed to warm to room temperature.

5.4.2 Phosgene Determination

Approximately 5ml of purified phosgene in ODCB was collected in a 10ml syringe. The volume was accurately determined by transferring the solution to a flamed dried 10ml graduated cylinder equipped with a septum. Equal portions of the phosgene solution were subsequently transferred into two dry Erlenmeyer flasks via canula. Sodium Iodide in dry acetone (NaI, 0.65M) was syringed into the phosgene solution with a separate dry syringe for each sample. A 2:1 mole ratio of NaI to $COCl_2$ was added, assuming a 50% yield of phosgene (Figure 5.7). The resulting I_2 was titrated using Sodium Thiosulfate Pentahydrate solution in distilled water ($Na_2S_2O_3 \cdot 5H_2O$, 0.53M) (59).

$$COCl_2 + 2NaI \longrightarrow I_2 + NaCl + CO$$

$$NaS_2O_3 \cdot 5H_2O + I_2 \longrightarrow 2NaI + NaS_4O_6 + 10\ H_2O$$

Figure 5.7 – Phosgene titration reactions.

5.4.3 Polyamine Phosgenation

The anhydrous phosgene/ODCB solution (100ml, 0.0672mol) was injected into a 1L five-necked reaction kettle (Ace glass, medium pressure glass reactor) immersed in an ice bath. Labeled polyamine (4.12g, 0.021mol - based on methylene dianiline) was dried

overnight at 50°C under vacuum (~1mmHg). The dried polyamine was heated to 90°C and dissolved in 27 times its weight of ODCB (~120ml). The solution turned golden, but some white and dark insoluble particulates were present. The solution was slowly transferred via canula into the reaction kettle with very rapid stirring; an orange/white slurry immediately formed in the flask. Care was taken to ensure that the polyamine solution streamed directly into the phosgene/ODCB solution. This prevents polyamine adherence to the walls of the kettle, which results in yield loss. The reaction kettle was removed from the ice bath and immersed into a silicone oil bath at room temperature. The reaction kettle was slowly heated to 70°C over a period of one hour. Upon reaching 70°C, the kettle was rapidly heated to 180°C and maintained at this temperature for thirty minutes. The mixture turned from a dark greenish gold at 120°C, to yellow at 160°C, to gold at 180°C. HCl gas was released slowly through a pressure release valve attached to the kettle after thirty minutes at 180°C. It took approximately two minutes to release the pressure at a slow enough rate so that solvent could not exit the reactor. The kettle was taken out of the bath and purged for thirty seconds with nitrogen gas to release additional HCl and phosgene. The reaction kettle was allowed to cool to room temperature with moderate stirring. While cooling, the product turned from gold to light brown. Some particulates formed in the solution during the cooling. The product was purified by vacuum filtration under a flowing N_2 blanket.

Vacuum distillation was performed to remove ODCB at 0.1mmHg at 60^{o}C. The temperature was raised in increments of ten degrees until condensation was no longer

observed. The product was a greenish/brown liquid. A ten-minute heat treatment was performed in a silicon bath at 200-205°C to remove residual HCl, $COCl_2$, and breakdown any isocyanate dimers. During the heat treatment, nitrogen was gently blown through the flask every two minutes for a maximum of ten seconds. After the second or third nitrogen purge the product turned from greenish brown to golden brown. The product was stored in a dry dessicator under N_2.

5.5 PMDI CHARACTERIZATION TECHNIQUES

5.5.1 Isocyanate Content Determination

Isocyanate content was determined in accordance with ASTM D 5155-91 section C (58). The titration was performed at one-tenth of the scale indicated in the standard procedure.

5.5.2 Molecular Weight Determination

M_n and M_w were determined by gel permeation chromatography (GPC). A small amount of pMDI (0.05g) was dissolved in dry $CHCl_3$ (1ml) and reacted with an excess of diethylamine for 30 minutes (1.0ml). The resulting urea derivative was rotovaped and the solid was dissolved in tetrahydrofuran (THF) to form a yellow solution. The urea derivative was passed through three columns of 500, 100 and 100 Angstroms at 40°C with a Waters 510 HPLC pump. The GPC was equipped with a Viscotek Differential Viscometer and Waters 410 Differential Refractometer. Molecular weight was calculated utilizing universal calibration with known standards. The molecular weight of pMDI was corrected for urea derivativization.

5.5.3 Isomer Ratio Determination

A portion of the pMDI-^{13}C, ^{15}N (~0.05g) was dissolved in dry $CHCl_3$ (~1ml). A 1μL sample was injected into a HP 6890 Series gas chromatograph. The parameter for analysis were:

Column: Model No. HP 19091 J-413, Capillary 30.0m x 320μm x 0.25μm nominal

Oven: 230°C for 10 minutes followed by a ramp of 30°C minute to 300°C

Pressure: 51.2 kPa

Flow: 0.7 ml/min

Split Ratio: 50.0:1

Detector: Flame Ionization

5.6 RESULTS AND DISCUSSION

Labeled aniline was reacted with paraformaldehyde to form polyamine. Polyamine was produced with a 74% yield based on the assumption that every mole of formaldehyde formed one mole of methylenedianiline. The product was a yellow gelatinous solid that turned brown when vacuum distilled above its melting point (84°C). The polyamine had

to be heated to 100°C to fully dissolve in ODCB. Below that temperature small amounts of brownish, possibly higher molecular weight material would not dissolve.

Chlorine gas was reacted with ^{13}C labeled carbon monoxide to form phosgene (57% based on moles of carbon monoxide). The product was clear within the gas and liquid state within the reaction kettle. Yield was calculated based on titration described in the experimental section. It was found that 150ml of ODCB gave the best overall yield.

Phosgene/ODCB solution was added into a one-liter five-necked kettle immersed in an ice bath. Dried ^{15}N polyamine (4.12g, .021mol) was dissolved in ODCB and added to the phosgene as described in section 5.3.3. 5.06g of pMDI was formed (100% yield based on monomer conversion). GC analysis showed 95% of the 4,4'-isomer and 5% of the 2,4'-isomer based on areas in the chromatogram; no response factors were used. No 2,2' isomer was observed (Figure 5.6).

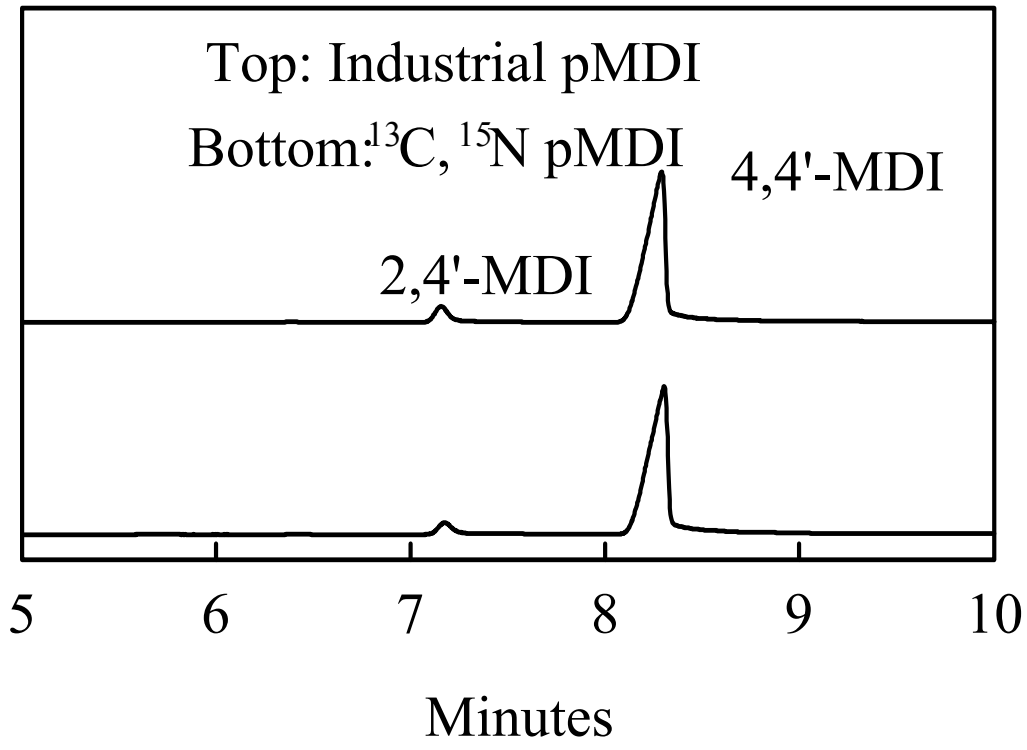

Figure 5.8 – Gas chromatogram of ^{13}C, ^{15}N, - pMDI. Higher polyisocyanates are not detected with this method.

The molecular weight of the pMDI-^{13}C, ^{15}N was determined to be M_n= 353, M_w= 378. The r^2 of the GPC calibration curve was 99.8%. Figure 5.7 shows the GPC chromatogram along with an industrial pMDI preparation.

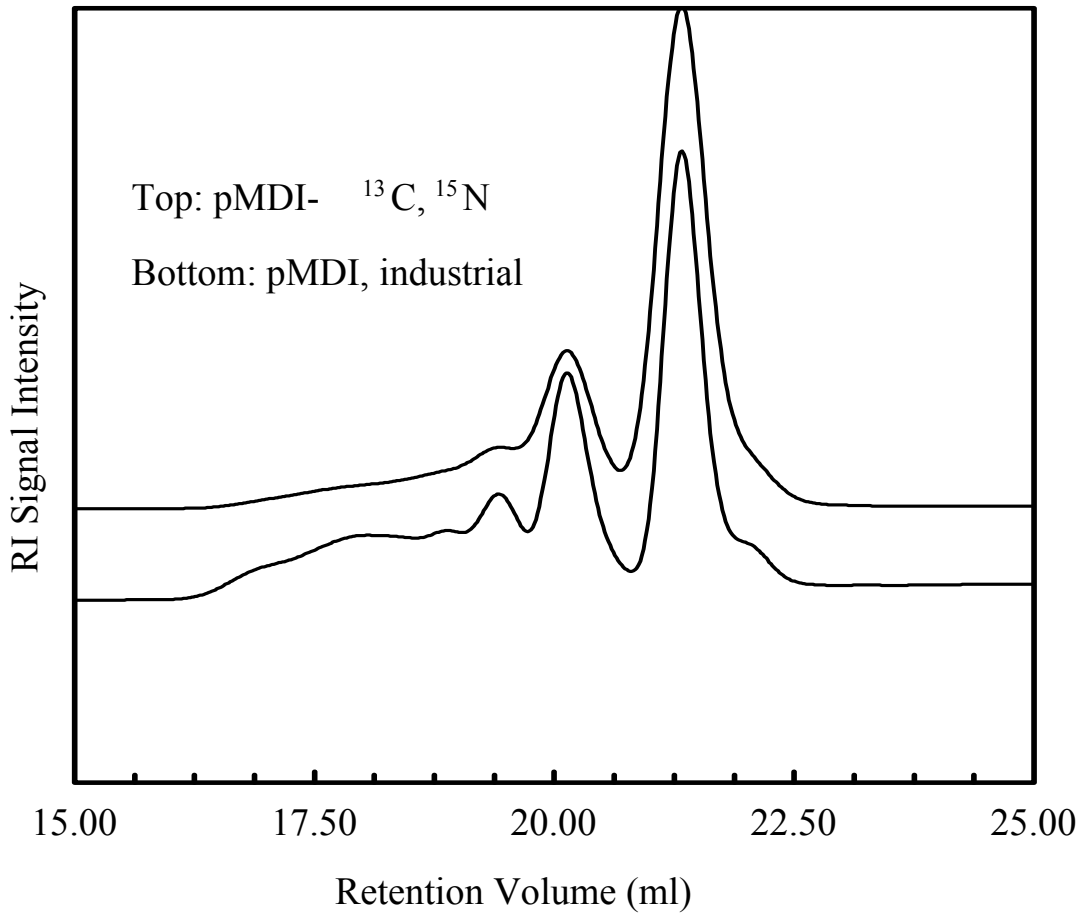

Figure 5.9 – GPC chromatogram of doubly labeled pMDI (top) vs. an industrial pMDI OSB core resin.

It can be seen that the molecular weights were very similar, but pMDI-^{13}C, ^{15}N had more monomer and less high molecular weight material. Two possible reasons for this could be; 1) Differences in the polyamine condensation forming the backbone of the pMDI adhesive. The industrial resin could contain more tri-, tetra, and higher weight polyamines. 2) In industrial applications, monomer is distilled out of the pMDI for use in higher margin applications, yielding a lower ratio of monomer to higher molecular weight constituents.

Figure 5.10 shows the proton spectra of the pMDI-^{13}C, ^{15}N and the industrial preparation. The figure shows the similarity between the two adhesives. A slight amount of impurities are seen in the pMDI-^{13}C, ^{15}N spectra. GC analysis showed no impurities. Figure's 5.10 and 5.11 illustrate solution NMR spectra of the pMDI-^{13}C, ^{15}N and industrial products. Deuterated chloroform was the solvent for all spectra.

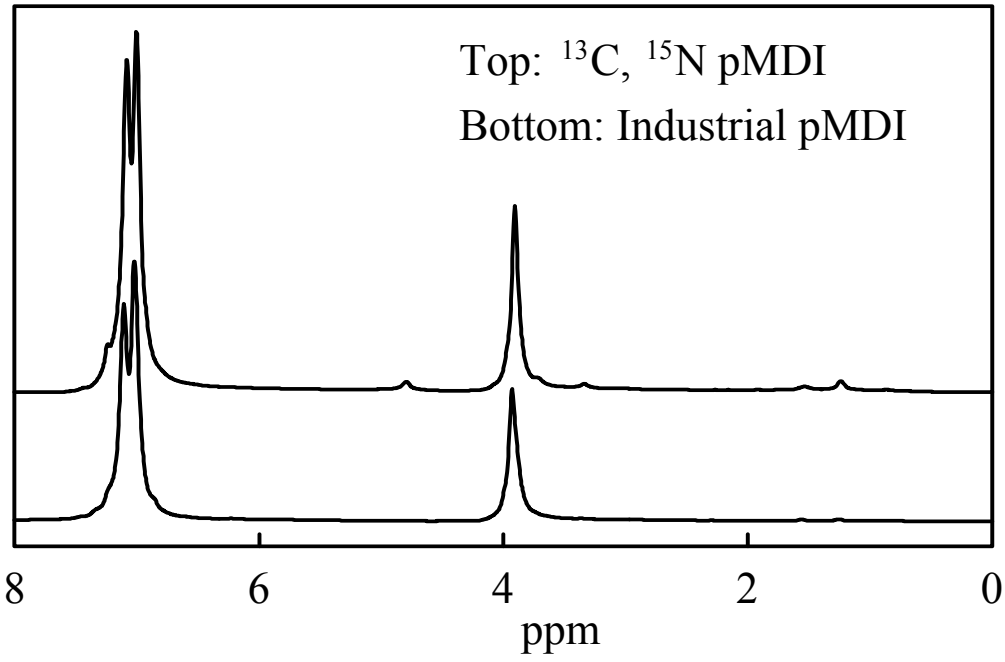

Figure 5.10 – Proton spectrum of synthesized doubly labeled pMDI vs. industrial pMDI in deuterated $CHCl_3$.

Figure's 5.11 illustrate the ^{13}C spectra's of pMDI-^{13}C, ^{15}N and industrial pMDI. In pMDI-^{13}C, ^{15}N, the isocyanate carbon at 125 ppm dominates the spectra. This is due to the ^{13}C label. These spectra show that pMDI-^{13}C, ^{15}N is representative of the industrial material.

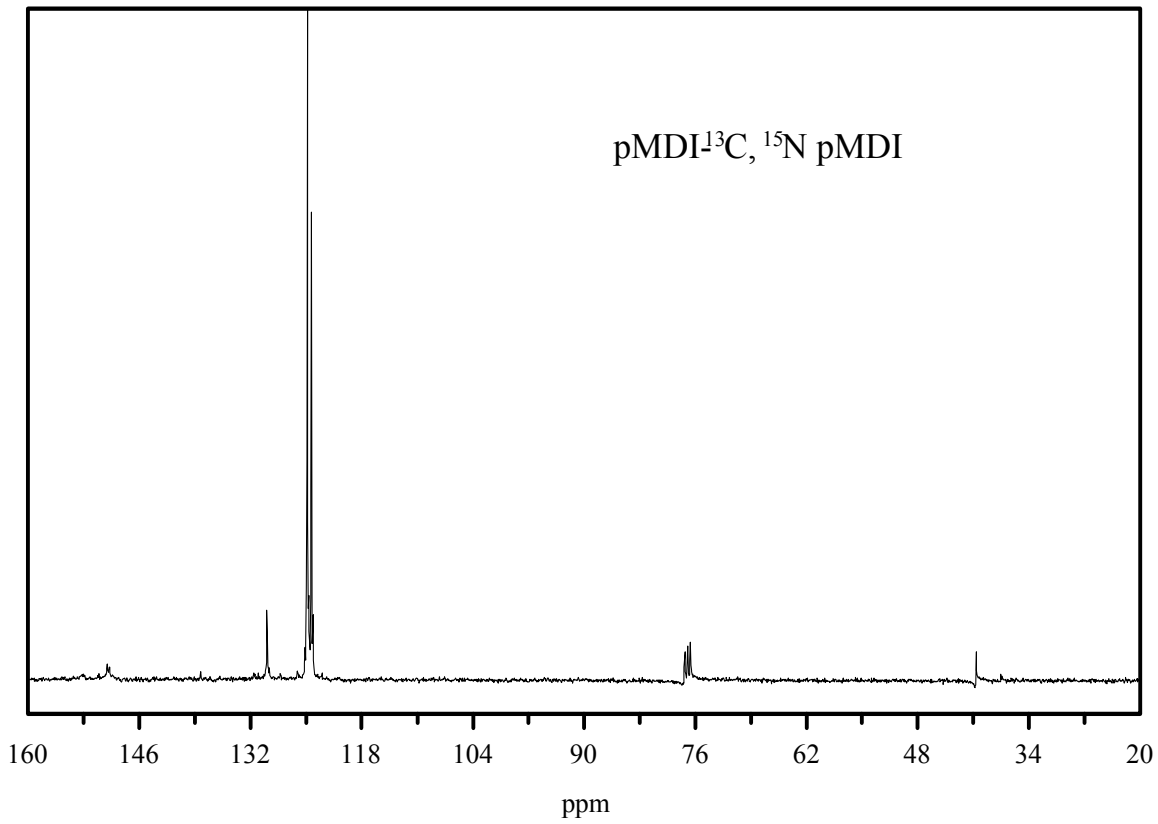

Figure 5.12 – Spectra of pMDI-^{13}C, ^{15}N referenced to deuterated chloroform.

It can be seen in the labeled spectra the magnitude of the labeled isocyanate peak at 124 ppm. The aromatic carbon peak is much smaller in magnitude without the label at 130 ppm. Some carbonyl is present at approximately 150 ppm, indicating a small amount of moisture contamination present during the reaction process. Comparing to the spectra of industrial pMDI it is similar, except for this contamination and the magnitude of the isocyanate carbon at 124ppm.

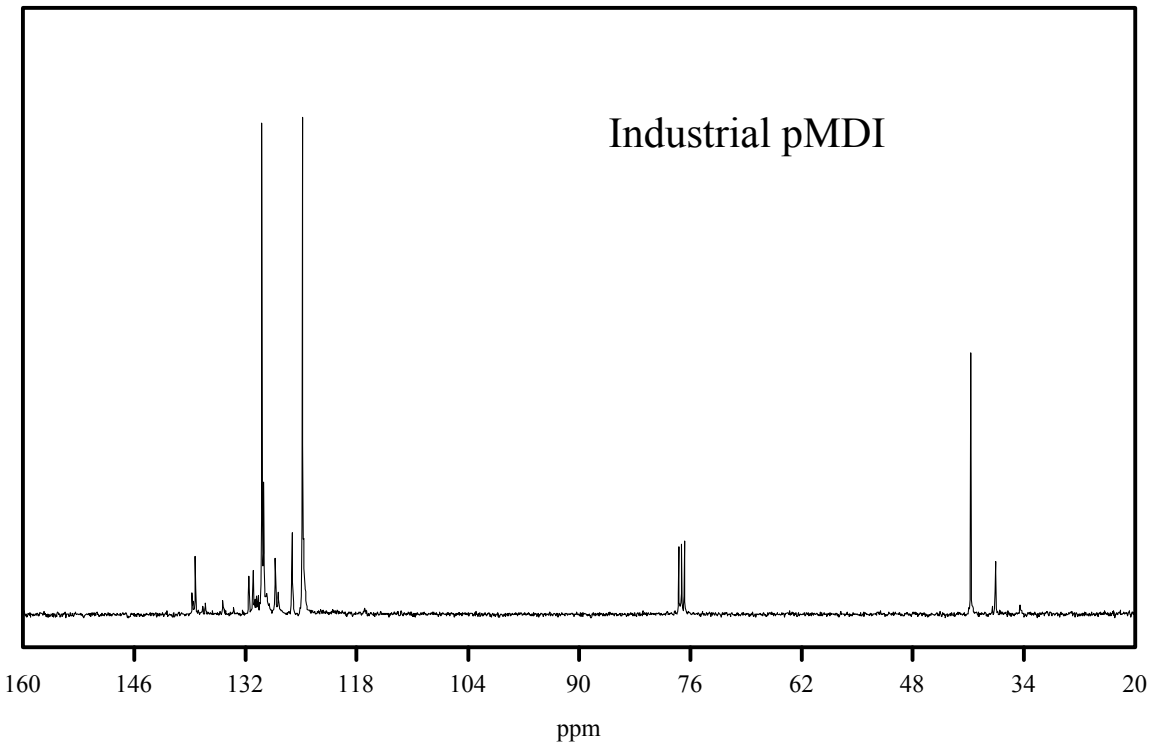

Figure 5.12 – Spectra of industrial pMDI referenced to deuterated chloroform.

Figure 5.12 illustrates the spectra of an industrial pMDI of an OSB formulation. The isocyanate carbon peak is located at 124 ppm and the aromatic carbons are located in that region between 124 ppm and 132 ppm. The methylene carbon resonance can be seen between 37 and 41 ppm. Unlike the labeled pMDI, the industrial shows no indication of carbonyls.

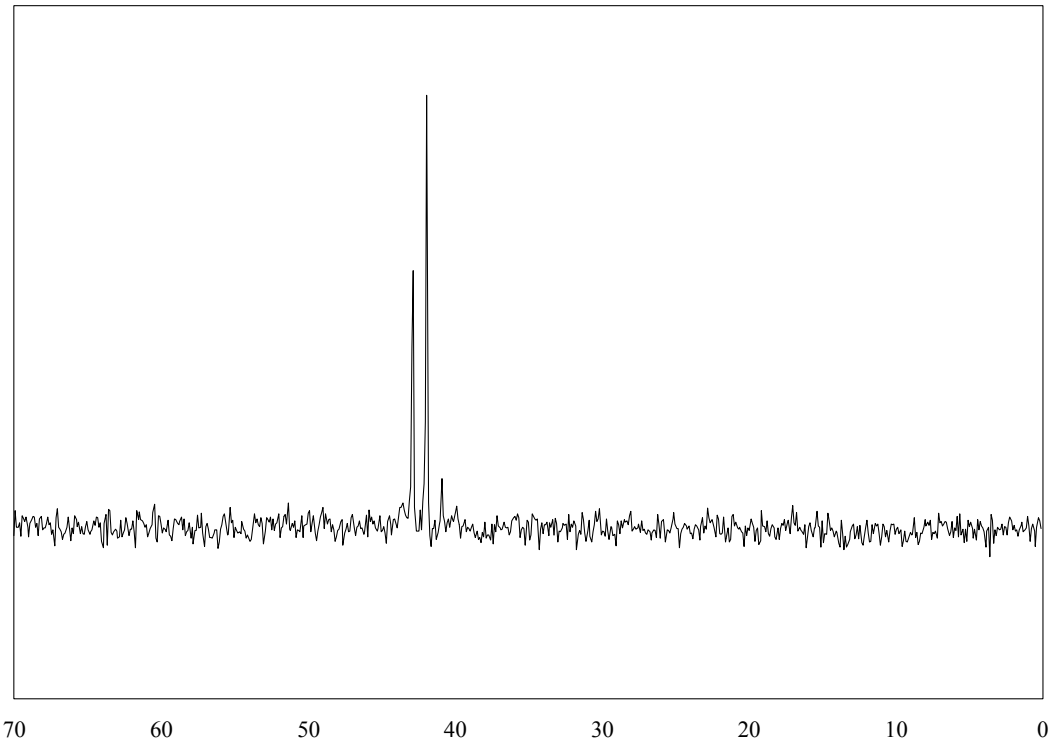

Figure 5.13 – ^{15}N spectra of pMDI-^{13}C , ^{15}N referenced to 15N glycerin.

Figure 5.13 illustrates the spectra the labeled isocyanate. No assignments were attempted and this spectrum is presented as a record for future reference.

- **Discussion of pMDI Chlorine Contamination**

Figure's 5.14 and 5.15 illustrate proton and carbon spectra of pMDI containing chlorine contamination. In the typical proton spectra, pMDI resonates at 7.2 (aromatic) and 4.0 ppm (methylene bridge) as shown in Figure 5.10. Contamination was identified in the proton spectra between 4.2 and 5.1 ppm. In the carbon spectra, contamination was identified between 60 and 70ppm. These contaminates were identified by reference to an on-line spectra library after analysis by GC/MS. It was found that 4% of the chlorine/ODCB solution was contaminated before the polyamine phosgenation. The main contaminates according to the GC/MS library were 1,1,2,3,4,5,6-heptachlorocyclohexane, 1,2,3,3-tetrachloro 1-propene, 1,2,3-tricholorbenzene and 1,2,4-trichlorobenzene. Proton and carbon NMR didn't show the tri-chlorobenzene well, due to the overlap with ODCB. Evidently, metal ions from either the chlorine lecture bottle or the lecture-bottle control valve were catalyzing a reaction between ODCB and chlorine. Chlorine from two different lots and two different types of lecture bottle control valves were compared and all ended up with the same relative amounts of chlorine contaminates. A phosgene purification step was added into the synthesis procedure (section 5.3.2) to eliminate these contaminates.

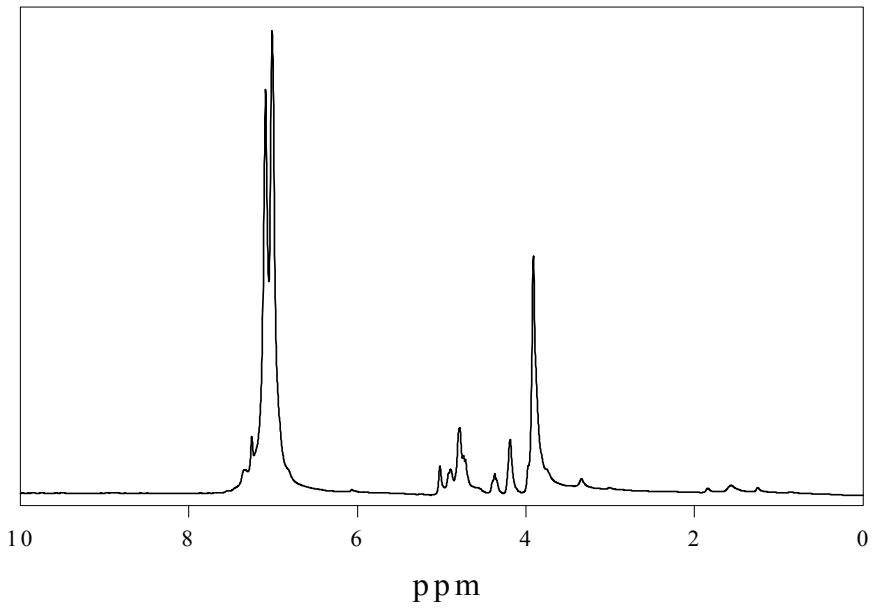

Figure 5.14 – Proton Spectrum of Synthesized pMDI Containing Chlorine contaminates at 4.2 and 5.1 ppm

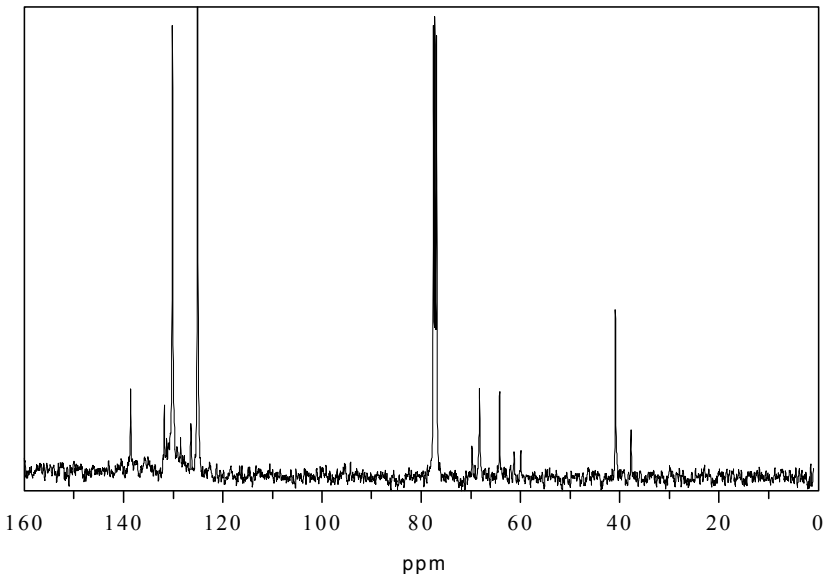

Figure 5.15 – ^{13}C Spectra of pMDI Containing Chlorine Contamination at 60 and 70 ppm

5.7 CONCLUSIONS

PMDI-^{13}C, ^{15}N was synthesized for use in solid-state NMR wood composite studies. Optimizations of the phosgene synthesis and phosgenation reaction were performed.

- **Phosgene Synthesis**

  Optimization of the phosgene reaction included:

  1) Purification of phosgene to eliminate chlorine contaminates
  2) Performing all steps in anhydrous conditions

These changes improved the phosgene yield to 57% compared to 45% by Zhou and Frazier (58).

- **Phosgenation of Polyamines**

The following steps were added to Zhou and Frazier's work:

1) Changed reaction kettle to special high pressure reaction flask with adaptors that facilitate easier injections, canula transfers and better seal to prevent moisture contamination.
2) Adjusted the vacuum filtration of pMDI from direct pouring in the flask where moisture could reduce yield to complete anhydrous conditions
3) Adjusted reaction from 40 minutes at 180^{o}C to method described in section 5.3.3

These changes resulted in 100% yield based on converting methylene dianiline into 4,4'-MDI monomer.

Appendix A

Preparation of ^{15}N, ^{13}C pMDI Laminated Flake Composites for Future Solid-State NMR Studies

Introduction

The double-labeled adhesive described in chapter 5 was intended for solid-state NMR studies that are not included in this thesis. However, the laminated flake composites intended for solids NMR analysis were prepared in this work, and this process is described as a record of the detailed procedure.

Preparation

Clear-grained 5.12 cm (2") x-sections of pine and poplar were disc flaked, leaving a radial surface. The flakes were conditioned to 6% EMC in a desicator over a saturated salt solution of chromium trioxide for one month. Samples were cut into 2.54cm x 2.54cm (1" x 1") sections and weighed before making 2-ply composites using the double-labeled pMDI.

The double-labeled pMDI described in chapter 5 was stored in a 25 ml round bottom flask under dry nitrogen. A spatula was dipped into the liquid pMDI and dabbed onto the wood flakes. A total of 40 to 45 drops of labeled resin was distributed over both bonding surfaces; this resulted in a resin content of approximately 15% OD wt. After adhesive application, the two flakes were consolidated and pressed in a 15.24cm x 15.24cm (6" x 6") press. These composites were pressed at 4.48 MPa (650 psi) at varying temperatures and times. Twenty-two 2-ply composites were made and the pressing conditions are given in Table 1. The composites were stored in a under vacuum in desicator filled with drierite.

REFERENCES

1. Frink, J. W. and H.I. Sachs. 1981. Urethane chemistry and applications. In ASC Symp. Series No. 172, Washington D.C. 285.

2. Johns, W.E. 1989. The chemical bonding of wood. In Wood Adhesives Chemistry and Technology. Marcel Dekker, Inc. New York, N.Y. 2: 75-96.

3. Hawke, R.N., B.C.H. Sun and M.R. Gale. 1992. Effect of fiber mat moisture content on strength properties of polyisocyanates-bonded hardboard. Forest Prod. J. 42(11/12): 61-68.

4. Hawke, R.N., B.C.H. Sun and M.R. Gale. 1993. Effect of fiber mat moisture content on physical properties of polyisocyanates-bonded hardboard. Forest Prod. J. 43(1): 15-20.

5. Hawke, R.N., B.C.H. Sun and M.R. Gale. 1994. Effect of polyisocyanates level on the strength properties of wood fiber composite materials. Forest Prod. J. 44(3): 34-40.

6. Hawke, R.N., B.C.H. Sun and M.R. Gale. 1994. Effect of polyisocyanates level on physical properties of wood fiber composite materials. Forest Prod. J. 44(4): 53-58.

7. Twitchett, H. J. 1974. Chemistry and Production of Organic Isocyanates. In Chemistry of Cyanate, Chem. Soc. Rev., London Chem. Soc. 3(2): 209-230.

8. Wendler, S.L. and C.E. Frazier. 1995. The ^{15}N CP/MAS characterization of the isocyanate adhesive bondline for cellulosic substrates. J. Adhesion 50: 135-153.

9. Wendler, S.L. and C.E. Frazier. 1996. Effect of moisture content on the isocyanate/wood adhesive bondline by ^{15}N CP/MAS NMR. J. Appl. Polym. Sci. 61: 775-782.

10. Wendler, S.L. and C.E. Frazier. 1996. The effects of cure temperature and time on the isocyanate-wood adhesive bondline by 15N CP/MAS NMR. Int. J. Adhesion and Adhesives 16: 179-186.

11. Ni, J. and C.E. Frazier. 1998. On the occurrence of network interpenetration in the wood-isocyanate adhesive interphase. Int. J. of Adhesion and Adhesives 18: 81-87.

12. Ni, J. and C.E. Frazier. 1998. ^{15}N CP/MAS NMR study of the isocyanate/wood adhesive bondline. Effect of structural isomerism. J. Adhesion 66: 89-116.

13. Bao et al. 1999. Solid state NMR studies of polymeric diphenyl diisocyanate (PMDI) derived species in wood. J. Adhesion, 71: 377-394.

14. Marcinko et al. 1999. Exploring the physiochemical nature of PMDI wood structural composite adhesion. Forest Prod. J. 49(5):75-78.

15. Johns, W. E. et al. 1982. The effect of species and moisture content on the bonding efficiency of polymeric MDI isocyanate. Proceedings of the 16th W.S.U. Particleboard Symposium. 71.

16. Phanopoulos, C., C. Van Den Bosch and J. Vanden Ecker. Penetration of isocyanate (MDI) into wood and how this influences wood composite: some initial findings. Conference paper PG-44.

17. Deppe, Hans-Joachim. 1977. Technical progress in using isocyanate as an adhesive in particleboard manufacture. Proceedings of the 11th W.S.U. Symposium on Particleboard, 13-31.

18. Zicherman, Joseph B. 1975 Urethanes and composite wood products: A review and brief research results. Forest Prod. J. 25(6): 21-25.

19. Ulrich, Henri. 1996. Chemistry and Technology of Isocyanates. J. Wiley & Sons, New York. 385.

20. Galbraith, C.J. and W.H. Newman. 1992. Reaction mechanisms and effects with MDI isocyanate binders for wood composites. Proceedings of the Pacific Rim Bio Based Composites Symposium, Rotorua, New Zealand 130.

21. Ball, G.W. 1981. New opportunities in manufacturing conventional particleboard using isocyanate binders. Proceedings of the 15th W.S.U. Symposium on Particleboard. 265.

22. Rowell, Roger M. and D.W. Ellis. 1981. Bonding isocyanates to wood. In Urethane Chemistry and Applications, ACS Symposium Series, (172): 19.

23. Owens, N.L., W.B. Banks and H. West. 1988. FTIR studies of the "wood"-isocyanate reaction. J. of Molec.Struc. 175: 389-394.

24. Pizzi, A. 1994. Advanced Wood Adhesives Technology. Marcel Dekker Inc. New York, NY 1-14.

25. Clelak W. and Newman. 1991. Proceedings of the 25th W.S.U. Symposium on Particleboard. 205.

26. Weaver, W.F. and O.L. Noel. 1992. The isocyanate-wood adhesive bond. Pacific Rim Bio-Based Composites Symposium, 9-13 Nov. Rotorua, New Zealand: 143-153.

27. Epner, J. 2000. Personal communication of data produced at Dow Chemical.

28. Steiner, Paul R., S. Chow, and S. Vadja. 1980. Interaction of polyisocyante adhesive with wood. Forest Prod. J. 30(7): 21-27.

29. Koch, Peter. 1972. Utilization of the Southern Pines. Agricultural Handbook (420).

30. Panshin, A.J. and Carl de Zeeuw. 1980. Textbook of Wood Technology. 4th edition, McGraw-Hill, 444-446.

31. Wood Handbook: Wood as an Engineering Material. Agricultural Handbook, (72). Ch. 4.

32. Koch, Peter. 1985. Utilization of Hardwoods Growing on Southern Pine Sites. Agricultural Handbook (605).

33. Sjostrom, Eero. 1993. Chapter 4. Wood Chemistry Fundamentals and Applications. Second Edition, Academic Press.

34. Wise, Louis and Edwin C., Jahn. Wood Chemistry. 2nd edition, Reinhold Publishing, New York, NY 2: 1130.

35. Hillis, W.E. 1962. Wood Extractives. Academic Press, New York, 331.

36. Rowell, Roger M. 1983. The Chemistry of Solid Wood. American Chemical Society, Cellulose, Paper and Textile Division. III. Series. 76,80.

37. Ebewele, Robert, B.H. River and J.A. Koutsky. 1979. Tapered Double Cantilever Beam Fracture Tests of Phenolic-Wood Adhesive Joints. Wood and Fiber 11(3): 197-213.

38. Scott, C.T., B.H. River, and J.A. Koutsey. 1992. Fracture Testing Wood Adhesives with Composite Cantilever Beams. J. of Testing and Evaluation, 20(4): 259-264.

39. River, B.H. and E.A. Okkonen. 1993. Contoured Wood Double Cantilever Beam Specimen for Adhesive Joint Fracture Tests. (21): 1, 21-28.

40. ASTM D3433-93, Standard test method for fracture strength in cleavage of adhesives in bonded metal joints. Annual Book of ASTM Standards Vol.15.06, 212-218.

41. Lim, W.W.Y. Hatano and H. Mizumachi. 1994. Fracture toughness of adhesive joints. I. relationship between strain energy release rates in three different fracture modes and adhesive strengths. J. Appl. Polym. Sci. (52): 967-973.

42. Schmidt, R. 1997. Fracture toughness testing of bonded wood assemblies. PhD. Thesis. 117-138.

43. Gagliano, J. M. and C.F. Frazier. 2001. Improvements in the fracture cleavage testing of adhesively-bonded wood. Wood and Fiber Sci. 33(3): 377-385.

44. Gordon, J.E. 1976. Crack stopping. The new science of strong materials. 2nd edition. Penguin. 101–128.

45. Ripling, E.J. and S. Mostovoy. 1971. Fracture mechanics: A tool for evaluating structural adhesives. J. Adhesion (3): 107-123.

46. ASTM D905 - 89, Strength properties of adhesive bonds in shear by compression loading. Annual Book of ASTM Standards Vol. 04.09, 26-29.

47. Rakestraw, M.D., M.W. Taylor and D.A. Dillard. 1995. Time dependent crack growth and loading effects on the interfacial and cohesive fracture of adhesive joints. J. Adhesion, (55): 123-149.

48. Gray, V.R. 1962. The wettability of wood. Forest Prod. J, 12(9): 452- 461.

49. Good, Robert J. 1992. Contact angle, wetting and adhesion: a critical review. J. Adhesion Sci. Tech. 6(12): 1269-1302.

50. Hse, Chung-Yun. 1972. Wettability of southern pine veneer by phenol formaldehyde wood adhesives. Forest Prod. J. 22(1): 51-56.

51. Nguyen T. and W.E. Johns 1979. The effects of aging and extraction on the surface free energy of douglas fir and redwood. Wood Sci. Tech. 13: 29-40.

52. Gardner D.J. 1996. Application of the Lifshitz-van der Waals acid-base approach to determine wood surface tension components. Wood Sci. Tech. 28(4): 422-428.

53. Shen, Q., J. Nylund, J.B. Rosenholm. 1998. Estimation of the surface energy and acid-base properties of wood by means of wetting method. Holzforshung (52): 521-529.

54. Eley, D. D. 1961. Thermodynamic adhesion. In Adhesion, Oxford university press. 39-67. f

55. Kinloch, A. J. 1987. In Adhesion and Adhesives: Science and Technology. Chapman and Hall, London; New York. 82-86.

56. Zhou, X. and C.E. Frazier. 2001. Double labeled isocyanate resins for the solid-state NMR detection of urethane linkages to wood. Int. J. Adh. & Adhesives, 21(3): 259-264.

57. Phosgene. 1991. In Encyclopedia of chemical technology 4th edition. Wiley-Interscience, New York. 18.

58. ASTM D5155-91. Section C. Annual Book of ASTM Standards. 15.05:357-361.

59. Rush, C.A. and C.E. Danner. Analysis of liquid phosgene. In Proceeding of the 112th Meeting of the American Chemical Society 9 October 1947. New York, N.Y., 644, 1947.

60. Gardner, D.J., Tze W.T. and Shi, S.Q. 1999. Surface energy characterization of wood particles by contact angle analysis and inverse gas chromatography. In Advances in Lignocellulosics Characterization. TAPPI Press. 12:263-293.

61. Johnson, S.E. 1990. Thesis. Virginia Polytechnic Institute & State University.

VITA

Mike Malmberg was born to Wally and Beverly Malmberg on January 25, 1971. He was born and raised in Ironwood, Michigan graduating from Luther L. Wright High School in 1989. Mike spent four years after graduation in the United States Marine Corps. After military duty he studied at Michigan Technological University where he attained a B.S. in Wood Science. After leaving VPI, Mike married Lynn Patricia Simon and they currently reside in Hungry Horse, MT. Mike has three stepchildren: Brette, Devon and Brooke Cady. Mike and Lynn have recently had a baby boy: Peyton Michael Malmberg. His mother, Beverly Sublett also lives with them. Mike is in his third year as a tech service representative with Borden Chemical Inc.